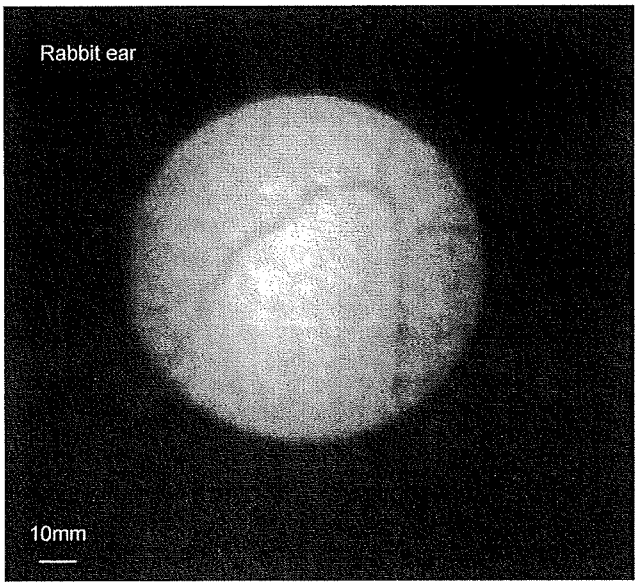

Fig. 6. An angiographic image of a rabbit ear. Due to filling of vascular beds with iodine-labelled microspheres of 15 μm in diameter, the 3rd vascular branch of 480 μm in bore is definitely observed.

are not yet optimized. Much better-quality images with higher spatial resolution and contrast are expected by optimizing these parameters. Moreover, upgrading of Compton X-ray system to increase the X-ray–photon yield is now in progress. The total yield presently obtained at the generating point is of the order of 10^7 photons/s at the maximum in 10 pps operation condition. This value is expected to be enhanced by at least two orders of magnitude [18]. This will enable us to obtain more distinctive real-time X-ray motion pictures of medical specimens using not only the HARP system but also an X-ray flat-panel detector, which is becoming popular in the medical imaging field due to its large detection area.

4. Conclusion

Laser-Compton X-rays were applied to fine and low-dose imaging of biological specimens. Due to the partial spatial coherence and quasi-monochromaticity of the Compton X-rays, fine structure in bones of a rat or a mouse and blood vessels with a contrast medium in a rabbit ear were successfully imaged using refraction-contrast and K-edge-contrast schemes, respectively. It was also found that a distinctive image could be taken by a single-shot picosecond Compton X-ray pulse using a highly sensitive HARP camera for the first time. Upgrading of the Compton X-ray system now in progress to increase X-ray yields will enable us to obtain more distinctive real-time X-ray images using not only the HARP system but also an X-ray flat-panel detector.

Acknowledgements

The authors would like to thank T. Shiraishi of NHK engineering service and T. Kawai and T. Atsumi of Hamamatsu photonics for their help in the data acquisition with the HARP system. This work was partially supported by the grant-in-aid for scientific research from the Japan society for the promotion of science (JSPS).

References

[1] H. Toyokawa, H. Ohgaki, S. Sugiyama, T. Mikado, K. Yamada, R. Suzuki, T. Ohdaira, T. Yamazaki, Nucl. Instr. and Meth. A 422 (1998) 95.
[2] R. Kuroda, H. Toyokawa, N. Sei, M. Yasumoto, H. Ogawa, M. Koike, K. Yamada, T. Nakajyo, F. Sakai, T. Yanagida, Int. J. Mod. Phys. B 21 (2007) 488.
[3] K. Yagi-Watanabe, M. Tanaka, F. Kaneko, K. Nakagawa, Rev. Sci. Instrum. 78 (2007) 123106.
[4] K. Yamada, N. Sei, H. Ogawa, M. Yasumoto, T. Mikado, Nucl. Instr. and Meth. A 528 (2004) 268.
[5] N. Oshima, R. Suzuki, T. Ohdaira, A. Kinomura, T. Narumi, A. Uedono, M. Fujinami, J. Appl. Phys. 103 (2008) 094916.
[6] T. Yamazaki, T. Noguchi, S. Sugiyama, T. Mikado, M. Chiwaki, T. Tomimasu, IEEE Trans. Nucl. Sci. NS-32 (1985) 3406.
[7] H. Ohgaki, T. Noguchi, S. Sugiyama, T. Mikado, M. Chiwaki, K. Yamada, R. Suzuki, N. Sei, T. Ohdaira, T. Yamazaki, Nucl. Instr. and Meth. A 375 (1996) 602.
[8] H. Toyokawa, T. Mikado, H. Ogawa, N. Sei, K. Yamada, M. Yasumoto, H. Ohgaki, N. Aoki, N. Kobayashi, in: Proceedings of the 2003 Particle Accelerator Conference, Portland, OR, USA, May 12–16, 2003, p. 713.
[9] F.E. Carroll, M.H. Mendenhall, R.H. Traeger, C. Brau, J.W. Waters, Am. J. Roentgenol. 181 (2003) 1197.
[10] F. Sakamoto, M. Uesaka, T. Yamamoto, T. Natsui, Y. Taniguchi, H. Sakane, D. Ishida, H. Nose, N. Kaneko, H. Sakai, T. Higo, M. Akemoto, J. Urakawa, M. Yamamoto, in: Proceedings of the 22nd Particle Accelerator Conference (PAC07), Albuquerque, NM, 2007, p. 2784.
[11] K. Sakaue, M. Washio, S. Araki, M. Fukuda, Y. Higashi, Y. Honda, T. Taniguchi, T. Terunuma, J. Urakawa, N. Sasao, in: Proceedings of the 11th European Particle Accelerator Conference (EPAC08), Genoa, Italy, 2008, p 1872.
[12] R.J. Loewen, SLAC Report 632 (2003).
[13] K. Mori, N. Sekine, H. Sato, D. Shimao, H. Shiwaku, K. Hydo, H. Sugiyama, M. Ando, K. Ohashi, M. Koyama, Y. Nakajima, J. Sychrotron Rad. 9 (2002) 143.
[14] H. Ikeura-Sekiguchi, R. Kuroda, M. Yasumoto, H. Toyokawa, M. Koike, K. Yamada, F. Sakai, K. Mori, K. Maruyama, H. Oka, T. Kimata, Appl. Phys. Lett. 92 (2008) 131107.
[15] H. Mori, K. Hyodo, E. Tanaka, M.U. Mohanmed, A. Yamakawa, Y. Shinozaki, H. Nakazawa, Y. Tanaka, T. Sekka, Y. Iwata, S. Handa, K. Umetani, H. Ueki, T. Yokoyama, K. Tanioka, M. Kubota, H. Hosaka, N. Ishikawa, M. Ando, Radiology 201 (1996) 173.
[16] H. Mori, E. Tanaka, K. Hyodo, M.U. Mohanmed, T. Sekka, K. Ito, Y. Shinozaki, A. Tanaka, H. Nakazawa, S. Abe, S. Handa, M. Kubota, K. Tanioka, K. Umetani, M. Ando, Am. J. Physiol. 276 (1999) H429.
[17] K. Tanioka, in: Proceedings of the ICFA workshop on Compton Sources for X/gamma Rays: Physics and Applications, Alghero, Italy, September 7–12, 2008.
[18] R. Kuroda,, H. Toyokawa, M. Yasumoto, H. Ikeura-Sekiguchi, M. Koike, K. Yamada, T. Yanagida, T. Nakajyo, F Sakai, in: Proceedings of the ICFA workshop on Compton Sources for X/gamma Rays: Physics and Applications, Alghero, Italy, September 7–12, 2008.

Nitric Oxide Release in Human Aortic Endothelial Cells Mediated by Delivery of Amphiphilic Polysiloxane Nanoparticles to Caveolae

Takehiro Nishikawa,*,† Norio Iwakiri,‡ Yoshiro Kaneko,‡ Akihiko Taguchi,† Kazuhito Fukushima,† Hidezo Mori,† Nobuhiro Morone,§ and Jun-ichi Kadokawa*,‡

National Cardiovascular Center Research Institute, 5-7-1, Fujishirodai, Suita, Osaka 565-8565, Japan, National Center of Neurology and Psychiatry, National Institute of Neuroscience, 4-1-1, Ogawahigashimachi, Kodaira, Tokyo 187-8502, Japan, and Graduate School of Science and Engineering, Kagoshima University, 1-21-40 Korimoto, Kagoshima, Kagoshima 890-0065, Japan

Received February 1, 2009; Revised Manuscript Received June 8, 2009

Microdomains such as lipid raft and caveolae are organized as functional compartments in plasma membrane of cells. In this study, we note the functional platform of caveolae with dual functions, internalization of external substances and cell signalings leading to nitric oxide release, and hypothesize that the switching of enzyme activity of endothelial nitric oxide synthase can be achieved by targeting caveolae with nanoparticles. We prepared polysiloxane nanoparticles and studied cellular uptake of the nanoparticles and its concomitant influence on the nitric oxide release in human aortic endothelial cells. We found that polysiloxane nanoparticles were endocytosed via caveolae in human aortic endothelial cells and that enhanced nitric oxide release was followed by the cellular uptake of the nanoparticles. Furthermore, we confirmed that endothelial nitric oxide synthase was activated during cellular uptake of the nanoparticles. These findings support our idea that delivery of the polymeric nanoparticles to endothelial cells can lead to the induction of nitric oxide release.

Introduction

With the recent progress in structural biology, it has been revealed that microdomains such as lipid raft and caveolae are organized as functional compartments in plasma membrane of cells.[1] Caveolae in particular are abundant in the plasma membrane of endothelial cells, occupying 15% of total cell volume and function as platforms for signaling and transporting.[2] In relation with pathology, it is pointed out that a lost function of caveolae is involved in various cardiovascular diseases such as vascular dysfunction, atherosclerosis, and hypertrophy.[3] For instance, hypertension is one of the risk factors for various cardiovascular diseases such as atherosclerosis, ischemic heart failure, stroke, and chronic renal failure. Blood pressure is controlled using antihypertensive drugs, which are the major medication for treating hypertension. Nitric oxide (NO) is a key substance in the vasorelaxation process and plays a crucial role in the regulation of blood pressure.[4] Direct control of nitric oxide (NO) production in vascular endothelium can be a novel strategy of the medication for hypertension and can lead to the improvement of endothelial functions.[5] NO molecules are released from vascular endothelium, are diffused to media, the outer layer of smooth muscle cells, and trigger the activation of soluble guanylate cyclase that leads to smooth muscle cell relaxation.[6] NO is synthesized by endothelial nitric oxide synthase (eNOS) that is embedded in caveolae and is activated by external stimuli such as bioactive substances and dynamic environmental factors.[7] Caveolae are characteristic flask-shaped invaginations of plasma membrane with diameters of 50−100 nm and work as functional platforms for internalization of extracellular materials (endocytosis) and cell signalings leading to NO production.[3]

In the past studies about vascular drug delivery, it was noted that caveolae can provide a possible pathway for drug delivery coupled with caveoli-mediated endocytosis.[8] To date, nanoparticles as drug carriers have been extensively studied with regards to delivery, drug loading, drug release, in vivo circulation, and toxicological properties.[9] However, whether such a nanoparticle cause effects on the functions of cells, tissues, and organ remains still unclear. Considering the endocytic pathways of cells, it is known that four basic mechanisms, macropinocytosis, clathrin-mediated endocytosis, caveolin-mediated endocytosis, and clathrin- and caveolin-independent endocytosis, are involved in pinocytosis (endocytosis in all mammalian cells).[10] Bioactive substances and serum proteins circulating in bloodstream have been found to be external stimuli for the activation of signal transduction. Although it was reported that artificial nanoparticles could influence a cell function of macrophages upon the association with lipopolysaccharide,[11] the artificial nanoparticles have not been considered and discussed in terms of the external stimuli as an input signal at specific membrane microdomain of cells for the activation of signal transduction, so far. Therefore, we have an interest in the influence of cellular uptake of nanoparticles on the signal transductions leading to the expression of cell functions. As the first attempt, we prepared nanoparticles from amphiphilic polysiloxane and studied cellular uptake of the nanoparticles and its concomitant influence on NO release in human aortic endothelial cells.

In this research, we chose polysiloxane as a polymeric material for the preparation of nanoparticles, because siloxane backbone with self-repair property is quite stable in physiological conditions[12] and nanoparticles of polysiloxane are expected

* To whom correspondence should be addressed. Tel.: 81-6-6833-5012 (T.N.); 81-99-285-7743 (J.-i.K.). Fax: 81-6-6872-7485 (T.N.); 81-99-285-3253 (J.-i.K.). E-mail: tnishi@ri.ncvc.go.jp (T.N.); kadokawa@eng.kagoshima-u.ac.jp (J.-i.K.).
† National Cardiovascular Center Research Institute.
‡ Kagoshima University.
§ National Center of Neurology and Psychiatry.

10.1021/bm900128x CCC: $40.75
Published on Web 07/07/2009

to be resistant to biological degradation in both extracellular and cytoplasmic environments. Silicone derivatives are known to be very attractive materials, because they exhibit low toxicity and unique physical properties. Therefore they have been widely used as versatile products such as foam stabilizer, rubber, paint, fiber, glass, and textile.[13] In spite of the usage of polysiloxane in wide fields, polysiloxane has not been studied so far in terms of polymeric materials for nanoparticles that are aimed at drug delivery system. Although biodegradable polymers have been extensively studied as polymeric materials for nanocarriers, a recent review article indicates the toxicological problems associated with degradation products of biodegradable polymeric carriers.[14] Polysiloxane has noteworthy properties with regard to degradation, stability and durability, based on a self-repair mechanism where silanol groups generated by the degradation of siloxane backbone can condense each other to form new siloxane bonds.[12] Polysiloxane with stability and inertness is expected to achieve reduced toxicity and longer circulation in terms of their usage as a drug carrier. Here, we describe nanoparticle formation of amphiphilic polysiloxane, cellular uptake of polysiloxane nanoparticles via caveolae of membrane microdomains, and influence of polysiloxane nanoparticles on cellular function; nitric oxide release in human aortic endothelial cells.

Experimental Section

Materials. Amphiphilic polysiloxane (Am-PAPS) was prepared by the method described in our previous report.[15] Am-PAPS was labeled with fluorescein thioisocyanate and was named Flu-Am-PAPS. Rabbit anti-caveolin-1 IgG was purchased from Sigma (St. Louis, MI). Mouse anti-eNOS IgG and mouse antiphospho-Ser1177-eNOS IgG was purchased from BD Transduction Laboratories (Franklin Lakes, NJ). Rabbit anti-fluorescein IgG was purchased from Molecular Probes (Eugene, OR). Anti-rabbit IgG conjugated with gold nanoparticles (5 nm in diameter) was purchased from GE healthcare. TRITC-labeled anti-rabbit IgG and TRITC-labeled anti-mouse IgG were purchased from Molecular Probes (Eugene, OR). HRP conjugated antimouse IgG was purchased from Cell Signaling Technology (Danvers, Mass). Mono-sulfo-*N*-hydroxy-succinimido nanogold (NANOGOLD) was purchased from Nanoprobes (Yaphank, NY). Gold nanoparticle labeled Am-PAPS (Au-Am-PAPS) was prepared by coupling NANOGOLD to the amphiphilic polysiloxane. All other reagents were purchased from Gibco, Nacalai Tesque, Sigma, or Wako Pure Chemicals unless otherwise indicated.

Nanoparticles Suspension. Aqueous suspension of each amphiphilic polysiloxane (Am-PAPS, Flu-Am-PAPS, or Au-Am-PAPS) was prepared by dispersing it (initial concentration: 1 mg/mL) into cell culture medium (EGM-2; Cambrex) and sonication with bath-type ultrasound washer (25 W and 40 kHz for 5 min). The suspension was passed through the membrane filters with the pore size of 0.45 μm (Millex-GV; Millipore) and 0.22 μm (Millex-GV; Millipore) for sterilization. Concentration of Flu-Am-PAPS was determined by fluorescence spectroscopy and was 0.1 mg/mL that was based on calibration with fluorescein-labeled sugar conjugated PAPS (1 mg/mL dissolved in EGM-2).

Measurements. The ^{1}H NMR spectra (600 MHz) were recorded using a JEOL ECA600 spectrometer. Fluorescence spectra for quantitative analysis were obtained on a fluorescence spectrometer (RF-5300 PC: Shimadzu) using a quartz cuvette (1 mm path length). The dynamic light scattering (DLS) measurement was performed on a Zetasizer 3000 (Malvern Instruments). Morphological study of nanoparticles was carried out by scanning electron microscope (Hitachi S-4100 electron microscope). The observation of plasma membrane and cytosol of human aortic endothelial cells was performed by a transmission electron microscope (Tecnai G2 *Sphera*, FEI, U.S.A.). Fluorescence imaging was performed on a IX-71 (Olympus) equipped with a fluorescence mirror unit, U-MNIBA3 (band-pass filter from 470 to 495 nm for excitation light and using a long pass filter from 510 to 550 nm for emission light) for the detection of fluorescein emission and U-MWIG3 (band-pass filter from 530 to 550 nm for excitation light and using a long pass filter >575 nm for emission light) for the detection of rhodamine emission. High-pressure mercury lamp (USH-1030 L: Olympus) was used as a light source for the fluorescence microscopy and was powered by a power supply (BH2-RFL-T3: Olympus).

Cell Culture Experiment. Human aortic endothelial cells (HAECs) were purchased as cryopreserved samples of third passage (Lot: 4F1350) from Cambrex, Wakersville, MD. The HAECs used in the experiment were fourth passage. Polystyrene dishes (ϕ35 mm, Iwaki) were filled with 2 mL of a supplemented culture medium (EGM-2; Cambrex) and equilibrated in a 37 °C, 5% CO_2 humidified incubator for 30 min before cell seeding. After the frozen cells were thawed at 37 °C, 70 μL of the cell suspension (8.0×10^5 cells/mL, viability: 85% (determined by trypan blue exclusion test)) were seeded in the culture dishes. The cell-seeded plates were placed in a 37 °C, 5% CO_2 humidified incubator. The HAECs were cultured for 72 h before the medium exchange with nanoparticle suspension. For fluorescence microscopy observation, the cells were rinsed with PBS (warmed at 37 °C), fixed by immersing into 10% formaldehyde neutral buffer solution (Nacalai tesque) at room temperature (22 °C) for 15 min and washed three times with PBS (Gibco). Fluorescence images used for the quantitative analysis of the cellular uptake of nanoparticles were taken at the constant exposure time to compare fluorescence intensity of the images at prescribed incubation time. Fluorescence images of the cells were taken by a fluorescence microscope (IX71; Olympus) equipped with a CCD camera (DP70; Olympus). To perform quantitative evaluation of fluorescence intensity, the fluorescence images were taken at the same exposure time (1/6.0 s). The exposure time was automatically measured by the operating software of DP70. The appropriate exposure time was chosen under the condition that over exposed images should be avoided to calculate fluorescence intensity of the images as correct as possible. The excess over exposure and under exposure could be prevented when the exposure time was set at 1/6.0 s that was measured when the HAECs exposed to Flu-Am-PAPS for 6 h were photographed by DP70. Fluorescence intensity of the incorporated nanoparticles of Flu-Am-PAPS was measured by integrating the fluorescence intensity observed at each pixel of the fluorescence images using image analysis software (Fluoview ver. 5.0; Olympus).

Cytotoxicity Assay. Cytotoxicity of polysiloxane nanoparticles were assessed using Cell Count Reagent SF (Nacalai Tesque, Kyoto) as a colorimetric indicator for living cells. HAECs were seeded in each well of 96-well plates and were incubated in a 37 °C, 5% CO_2 humidified incubator for 24 h before cytotoxicity assay. Cell number in each well was adjusted by stepwise 2-fold dilution of HAECs cell suspension. The cell number per well ranged from 5000 to 40000 cells. The total amount of the cell suspension including growth medium was 100 μL per well. The growth medium was replaced with 100 μL of a suspension of polysiloxane nanoparticle (1 mg/mL) for cytotoxicity testing. After 6 or 24 h incubation, each well was rinsed with 100 μL of growth medium to remove polysiloxane nanoparticles and was filled with 100 μL of fresh growth medium. Then, 10 μL of Cell Count Reagent SF solution containing WST-8 (5 mM),[16] colorimetric indicator, was added to each well to evaluate cell viability. HAECs were incubated with WST-8 for 4 h. WST-8 is converted to water-soluble formazan by an electron mediator coupled to the intracellular reduction of NAD^+. Absorbance of each well was measured at 450 nm using a microplate reader (Model 680, Bio-Rad, Hercules, CA). Cell viability was evaluated by the following equation: (cell viability) = (Abs for samples to be tested − Abs for blank)/(Abs for control − Abs for blank) × 100, "Abs" stands for absorbance of each well at 450 nm.

Immunostaining. To visualize the localization of caveolin-1 and endothelial nitric oxide synthase (eNOS) in HAECs, each antigen was stained by immunological method using primary antibodies (rabbit anti-caveolin-1 IgG; Sigma and mouse anti-eNOS IgG; BD) and fluores-

cence labeled secondary antibodies (TRITC labeled anti-rabbit IgG and TRITC labeled anti-mouse IgG; Molecular Probes). For immunostaining, cells were fixed by 10% formaldehyde neutral buffer solution (Nacalai tesque) at room temperature (22 °C) for 15 min and permeated with 0.1% PBS (pH 7.2, Gibco) solution of Triton X-100 (Sigma) for 5 min at 20 °C. After 1 h of blocking with 1% normal goat serum solution, HAECs were incubated with a primary antibody (200 times dilution with 0.1% normal goat serum solution) for 1 h. The HAECs treated with primary antibody were incubated with fluorescent dye labeled secondary IgG for 1 h. Fluorescence images of the cells were taken by a fluorescence microscope (IX71; Olympus) equipped with a CCD camera (DP70; Olympus) and confocal laser scanning microscope (FV 100; Olympus).

Transmission Electron Microscopy (TEM). Two types of specimens, ultrathin section and rapid-freeze, deep-etch, freeze-replica, were prepared for the observation of fine structure of plasma membrane and cytosol in cells using transmission electron microscopy. HAECs were grown on carbon-coated sapphire glass with a diameter of 5 mm for 2 days after inoculation. Specimens for ultrathin section were prepared by the following method. For the TEM observation of polysiloxane nanoparticles in caveolae, HAECs were exposed to gold nanoparticle labeled Am-PAPS (Au-Am-PAPS) dispersed in growth medium (EGM-2) for 3 h. After a 3 h incubation with Au-Am-PAPS, the HAECs attached on coverslips were washed with NaHCa buffer (30 mM HEPES, 100 mM NaCl, 2 mM $CaCl_2$, pH 7.3) and treated with chemical fixation reagent (2.5% glutaraldehyde (GA), 150 mM sucrose in PBS buffer). In the case of the immunodetection of caveolae in HAECs, HAECs were fixed with NaHCa buffer containing 4% paraformaldehyde for 1 h, then treated with a quenching solution containing 50 mM lysine, 50 mM glycine, and 50 mM ammonium chloride, and permeated with 0.1% NaHCa buffer solution of Triton X-100 for 1 min. After 1 h of blocking with 1% BSA solution, HAECs were incubated with a primary antibody to caveolin-1 (200 times dilution with 0.1% BSA solution) for 1 h. The HAECs treated with anti-caveolin-1 IgG were incubated with 10 nm colloidal gold conjugated anti-rabbit IgG (10 times dilution with 0.1% BSA solution) for 1 h and treated with PBS containing 2.5% glutaraldehyde for 15 min. These fixed specimens of HAECs were postfixed with Osmium (0.1%) in 0.1 M PBS buffer. The cells were rinsed with PBS and distilled water, dehydrated with ethanol, and embedded in epoxy resin (EPON 812, TAAB Laboratories Equipment Ltd., UK) by polymerization for 72 h at 70 °C. Ultrathin sections of the embedded HAECs were cut at thickness of 70 nm with an ultramicrotome (Reichert-Nissei Ultracut N, Nissei Sangyo Co., Tokyo, Japan), mounted on electron microscope grids, stained with uranyl acetate/lead citrate, and then observed by TEM (Tecnai G2 *Sphera*, FEI, USA).

Specimens for the rapid-freeze, deep-etch, freeze-replica were prepared by the following method.[17] After a 1 h incubation with fluorescein-labeled nanoparticles (Flu-Am-PAPS), the HAECs were washed with the mammalian ringer solution (155 mM NaCl, 3 mM KCl, 2 mM $CaCl_2$, 1 mM $MgCl_2$, 3 mM NaH_2PO_4, and 5 mM HEPES brought to pH 7.4 with NaOH, plus 10 mM glucose). Immediately after being unroofed from the apical cell membrane, the basal cell membrane was fixed for 15 min in 1% paraformaldehyde/0.25% glutaraldehyde in buffer A (70 mM KCl, 5 mM $MgCl_2$, 3 mM EGTA, 30 mM HEPES buffer adjusted at pH 7.4 with KOH) and washed with the NaHCa buffer for 10 min three times. To identify the nanoparticles attached to the undercoat structure of plasma membrane, the detached basal side of plasma membrane of HAECs was labeled by treating with a primary antibody against the fluorescein molecule and a secondary antibody conjugated with 5 nm diameter colloidal gold. The labeled specimen was further fixed in 2% GA buffer on ice for 15 min. The specimen was washed in distilled water for 1 min before rapid freezing. The coverslip attached to the basal side of the HAECs was set on the plunger tip of the rapid freezing device (Polaron, U.S.A.) with the cytoplasmic surface of the plasma membrane down. The coverslip was fallen onto a polished pure copper block, which was precooled by liquid helium. The frozen coverslip was immersed in liquid nitrogen and was transferred into the freeze etching shadowing chamber (Bal-Tec BAF060, Liechtenstein). The cytoplasmic surface was deeply etched and rotary shadowed with platinum/carbon at an angle of 22° from the surface and with carbon from the top. The replica was removed from the coverslip in aqueous solution of 1% hydrofluoric acid. After the replica was washed with distilled water, the replica was mounted on mesh copper grid coated with polyvinyl Formvar (Nisshin EM, Japan). Finally, the sample grid was observed by TEM.

Nitric Oxide (NO) Detection. NO detection was carried out by referencing the previous literature.[18] HAECs were exposed to Dulbecco's modified Eagle medium (phenol red free DMEM, Invitrogen) containing 50 μM diaminorhodamine-4 acetoxymethyl ester (DAR-4 M AM; Daiichi pure chemicals) for 10 min. The DAR-4 M AM loaded sample was washed with DMEM (1 mL) and filled with 2 mL of DMEM for post incubation. Post incubation was performed for 15 min in a 37 °C, 5% CO_2 humidified incubator. The sample was rinsed with DMEM (1 mL) twice and filled with 1 mL of DMEM. Then, the dish was fixed on a microscope stage with adhesive tape. Fluorescence images were captured to monitor NO release by fluorescence microscope (IX-71 equipped with a temperature controlled stage (Microwarm Plate, Kitazato Supply) and a CCD camera (DP-70) Olympus) after the addition of DMEM (in case of resting state or after the cellular uptake of nanoparticles) or DMEM solution of bradykinin (1 μM) (in case of stimulation). Image capture was carried out every 30 s by initial 180 s of monitoring, then every 60 s by the end of monitoring at 900 s.

Western Blotting. HAECs cultured on a plastic culture dish (Iwaki, ϕ35 mm) were lysed with 40 μL of RIPA lysis buffer (Rockland, Gilbertsville, PA) for 5 min at 4 °C and scraped from the dish surface with a cell scraper. The lysates were collected and then centrifuged to remove insoluble materials at 10000*g* for 20 min. The supernatant was collected in a test tube. Protein concentration in the supernatant was determined by the Bio-Rad Protein Assay (Bio-Rad Laboratories, Hercules, CA) based on the method of Bradford. The supernatant was mixed with Laemmli sample buffer (Bio-Rad, Hercules, CA) containing 5% (V/V) β-mercaptoethanol and heated at 100 °C for 2 min. The reduced protein solutions, including 2 μg of the extracted proteins, were loaded into each well of 5−20% gradient SDS-PAGE gel (e-PAGEL, ATTO, Tokyo). The gel was run at 20 mA constant current in an electrophoresis chamber (AE6500, ATTO, Tokyo) plugged with a power supply (AE8135, ATTO, Tokyo). The proteins on a gel were transferred to a PVDF membrane (Clear Blot Membrane-P, ATTO, Tokyo) at 140 mA in a semi-dry electrophoretic transfer cell (AE6678, ATTO, Tokyo). The PVDF membrane was blocked with a blocking buffer (Blocking One-P, Nacalai Tesque, Kyoto) for 30 min at 20 °C and then incubated with a primary antibody (1000 times dilution with Can-Get-Signal; solution 1; Toyobo, Osaka) to each target protein (eNOS, phosphorylated eNOS at Ser1177, β-Tubulin) overnight at 4 °C. The target protein transferred on the PVDF membrane was reacted with horseradish peroxidase (HRP) conjugated secondary antibody (Cell Signaling, Danvers, Mass; 1000 times dilution with Can-Get-Signal (solution 2)) for 1 h at 20 °C and detected using colorimetric detection reagent (Ez West Blue, ATTO, Tokyo). The reagent contains 3,3′,5,5′-tetramethylbendidine (TMB), colorimetric reagent, and hydrogen peroxide, substrate for HRP. TMB yields blue color when oxidized with hydrogen peroxide (catalyzed by HRP). Blue bands indicating the target proteins appeared on a PVDF membrane after a PVDF membrane was treated with Ez West Blue. Colorimetric intensity of the bands on a PVDF membrane was measured by image capture using a digital scanner (GT-X700, EPSON, Tokyo) and image analysis software (Fluoview ver. 5.0; Olympus, Tokyo).

Results and Discussion

Polysiloxane Nanoparticles. In our previous report[15] we synthesized a novel amphiphilic polysiloxane and found that the amphiphilic polysiloxane formed nanoparticles with diameters of several tens of nanometers in water. In addition to the

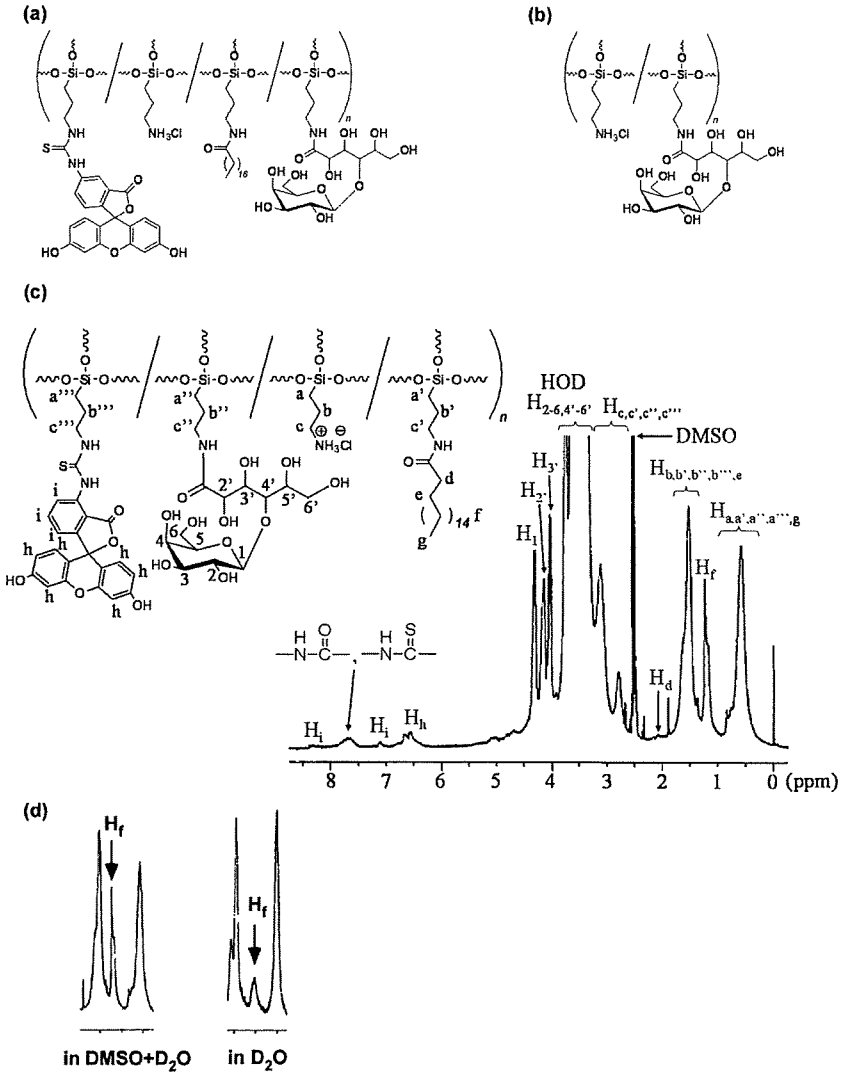

Figure 1. Chemical structure of (a) fluorescein-labeled amphiphilic polysiloxane (Flu-Am-PAPS) and (b) water-soluble sugar conjugated polysiloxane. (c) ^{1}H NMR spectrum of Flu-Am-PAPS in DMSO-d_6 (including a small amount of D_2O). Chemical shifts were referenced to DMSO (δ 2.5 ppm). (d) ^{1}H NMR signal of stearoyl group (H_f) observed in DMSO-d_6 (including a small amount of D_2O; left) and in D_2O (right).

amphiphilic polysiloxane, we obtained a fluorescence dye-labeled amphiphilic polysiloxane to track cellular uptake of the nanoparticles. We selected a fluorescein moiety as the fluorescent dye and synthesized the fluorescein-labeled amphiphilic polysiloxanes (Figure 1a) by using water-soluble poly(3-aminopropyl)siloxane (PAPS) having amino groups as a starting substrate as follows:[19] first, stearoyl groups as hydrophobic part and galactose moieties as hydrophilic part were introduced to PAPS in this order by the reactions of stearoyl chloride and lactobionolactone with the amino groups, respectively, giving an amphiphilic polysiloxane (Am-PAPS), and then, fluorescein-labeled polysiloxane (Flu-Am-PAPS: Figure 1a) was obtained by conjugation of fluorescein thioisocyanate to Am-PAPS. The molecular weight of PAPS as a polysiloxane backbone of Flu-Am-PAPS was measured by gel permeation chromatography with water as eluent and estimated to be 10300 g/mol (M_w/M_n = 1.41; pullulan was used as molecular weight standards). The substitution of amino groups in PAPS was estimated by ^{1}H NMR spectroscopy (Figure 1c) of the Flu-Am-PAPS; 2% of all amino groups was substituted for stearoyl group, 80% of those for galactose group, 4% of those for fluorescein and the rest of the amino groups were unreacted, that had been converted into the ammonium chlorides. For comparison, water-soluble sugar conjugated polysiloxane was synthesized (Figure 1b) by following the above method. The content of galactose moieties in the water-soluble polysiloxane was determined by ^{1}H NMR spectroscopy to be 43% (data not shown).

The amphiphilic polysiloxane (Am-PAPS/Flu-Am-PAPS) can form nanoparticles upon self-organization process in aqueous medium. Aqueous suspension of each amphiphilic polysiloxane was prepared by dispersing it (1 mg/mL) into cell culture medium for human aortic endothelial cells. The particle size of nanoparticles of the amphiphilic polysiloxane was measured by dynamic light scattering (DLS) measurement. The DLS measurement demonstrated that the Flu-Am-PAPS formed nanoparticles with a z-average diameter of 79 nm (0.290 for polydispersity index) in pure water. The particle size ranged from 40 to 400 nm (Figure 2a). About 48% of the nanoparticles comprised the group of nanoparticles whose diameter is less than 100 nm that is close to the caveolae size. The SEM image (Figure 2b) shows that the amphiphilic polysiloxane forms nanoparticles with diameters ranging from several tens of nanometers to 200 nm in diameter (average: 66 ± 30 nm). The difference in particle size bewteen DLS and SEM is attributable to the sample conditions (wet or dry) in these measurements.

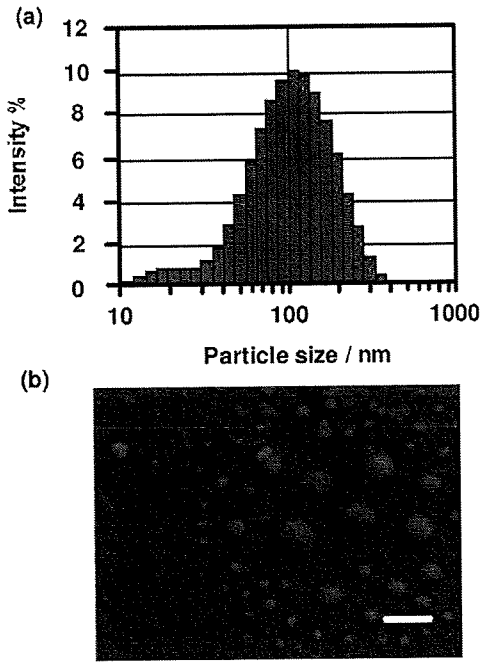

Figure 2. Particle size and morphology of nanoparticles of fluorescein-labeled amphiphilic polysiloxane (Flu-Am-PAPS). (a) Particle size histogram of nanoparticles of Flu-Am-PAPS. The nanoparticles were dispersed in pure water. (b) SEM image of Flu-Am-PAPS. Scale bar: 200 nm.

The nanoparticles had a slightly negative zeta potential (−0.9 mV) in the cell culture medium. The nanoparticle of Am-PAPS dispersed in phosphate buffered saline did not exhibit considerable change in particle size after one week storage at 37 °C (Figure S1a in Supporting Information). Furthermore, particle size measurement using DLS was carried out on the polysiloxane nanoparticles dispersed in cell culture medium containing 5% fetal bovine serum and found that one week storage of polysiloxane nanoparticles in serum containing culture medium at 37 °C caused little change in average particle size and particle size distribution (Figure S1b in Supporting Information). These data suggest that nanoparticles of Am-PAPS are stable in physiological condition. According to our recent report,[15] the NMR spectroscopy for the long alkyl side chains of the amphiphilic polysiloxane indicated that the signal intensity of protons in long alkyl chains become weak when the amphiphilic polysiloxane dissolved in D_2O was measured. Figure 1c shows that the signal observed around δ 1.25 ppm is ascribed to the protons of stearoyl chains attached to Flu-Am-PAPS and the signal intensity of the peak at δ 1.25 ppm of Flu-Am-PAPS dissolved in D_2O is weakened to the 76% of that of the peak at δ 1.25 ppm measured in DMSO (Figure 1d). The decrease in the intensity of the proton signal results from the restricted molecular motion of long alkyl chain and indicates that the molecular aggregation of Flu-Am-PAPS is driven by inter/intra hydrophobic association between stearoyl groups attached to the polysiloxane backbone.

Cellular Uptake of Nanoparticles by Human Aortic Endothelial Cells. Cellular uptake of the nanoparticles by HAECs was observed by fluorescence microscopy. HAECs were cultured for 72 h to obtain confluent culture of HAECs after cell suspension of HAECs was seeded on tissue culture dishes. At 72 h after cell seeding, cell culture medium was replaced with the polymer suspension of Flu-Am-PAPS. Then the HAECs were cultured in the polymer suspension for 15 min, 1, 3, 6, 24, 48, 72, and 144 h to monitor cellular uptake of the nanoparticles of Flu-Am-PAPS. The polymer suspension in cell culture dishes was exchanged daily during the incubation with Flu-Am-PAPS. Clearance of the incorporated nanoparticles from HAECs was observed after the nanoparticle suspension in culture dishes was replaced with EGM-2, growth medium for HAECs. For fluorescence microscopy observation, the cells were rinsed with 37 °C phosphate buffered saline (PBS), then were fixed by immersing into 10% formaldehyde neutral buffer solution at room temperature for 15 min and washed three times with PBS. Fluorescence images of the cells were taken by a fluorescence microscope equipped with a CCD camera at each incubation time. To evaluate cellular uptake of nanoparticles quantitatively, fluorescence intensity (F.I.) per image was determined by integrating the brightness at each pixel of fluorescence image using an image analysis software. The F.I. was normalized in a ratio of the F.I. at each incubation time over the F.I. at 6 h of incubation (the relative fluorescence intensity). The time course of the relative F.I. was plotted on the graph, Figure 3a (closed circles: uptake of nanoparticles; open circles: clearance of nanoparticles). HAECs incorporated progressively nanoparticles of Flu-Am-PAPS until 72 h of incubation and reached saturation thereafter until the end of observation at 144 h of incubation. Decline of F.I. after the removal of Flu-Am-PAPS from the cell culture dishes at 6 h of incubation indicates that the incorporated nanoparticles of Flu-Am-PAPS were gradually excreted from HAECs. However, 40% of the incorporated nanoparticles were still trapped in cytosol of HAECs at 138 h of post incubation (144 h of total incubation time). Meanwhile, the relative F.I. for the uptake dropped to only 2% of the control level (left bar in Figure 3b: 6 h at 37 °C) when HAECs were exposed to the nanoparticles at 4 °C of the incubation temperature for 6 h (middle bar in Figure 3b). Considerable cell detachment was not observed even after 6 h of the incubation at 4 °C. This means that cell culture of HAECs was maintained at a low culture temperature and the HAECs were alive. The temperature triggered dramatic decrease in the relative F.I. suggests that the nanoparticles are mainly incorporated into HAECs by endocytosis, not by adsorption to cell membrane. Endocytosis was restored after the HAECs exposed to low temperature environment were put back to the regular culture condition (cell culture at 37 °C). The reduced relative F.I. corresponding to the nanoparticle uptake at 4 °C increased to 90% of the relative F.I. that was measured after 6 h of incubation with Flu-Am-PAPS nanoparticles at 37 °C (left (incubation at 37 °C for 6 h) and right (incubation at 4 °C for 6 h and postincubation at 37 °C for 6 h) bars in Figure 3b). To ensure that the cellular uptake study was carried out under the condition that the dose of polysiloxane nanoparticles had little toxicity on HAECs, cytotoxicity of the polysiloxane nanoparticles in HAECs was evaluated by colorimetric cell viability assay using WST-8 as an indicator. Cell viability of HAECs was 95% when HAECs were cultured in the growth medium containing 1 mg/mL of Flu-Am-PAPS for 24 h. This suggests that the cellular uptake study was carried out under the condition that the polysiloxane nanoparticles did not exhibit cytotoxicity toward HAECs at 1 mg/mL of Flu-Am-PAPS.

Caveolae as Endocytic Pathway for Nanoparticles. Endocytosis is one of the important cell activities in internalization of various extracellular substances.[20] Endocytic pathways have been taken into account in targeted delivery of drug to vascular tissue. Caveolae are flask-shaped invaginations of cell membrane with diamters of 50−100 nm and are thought to function as

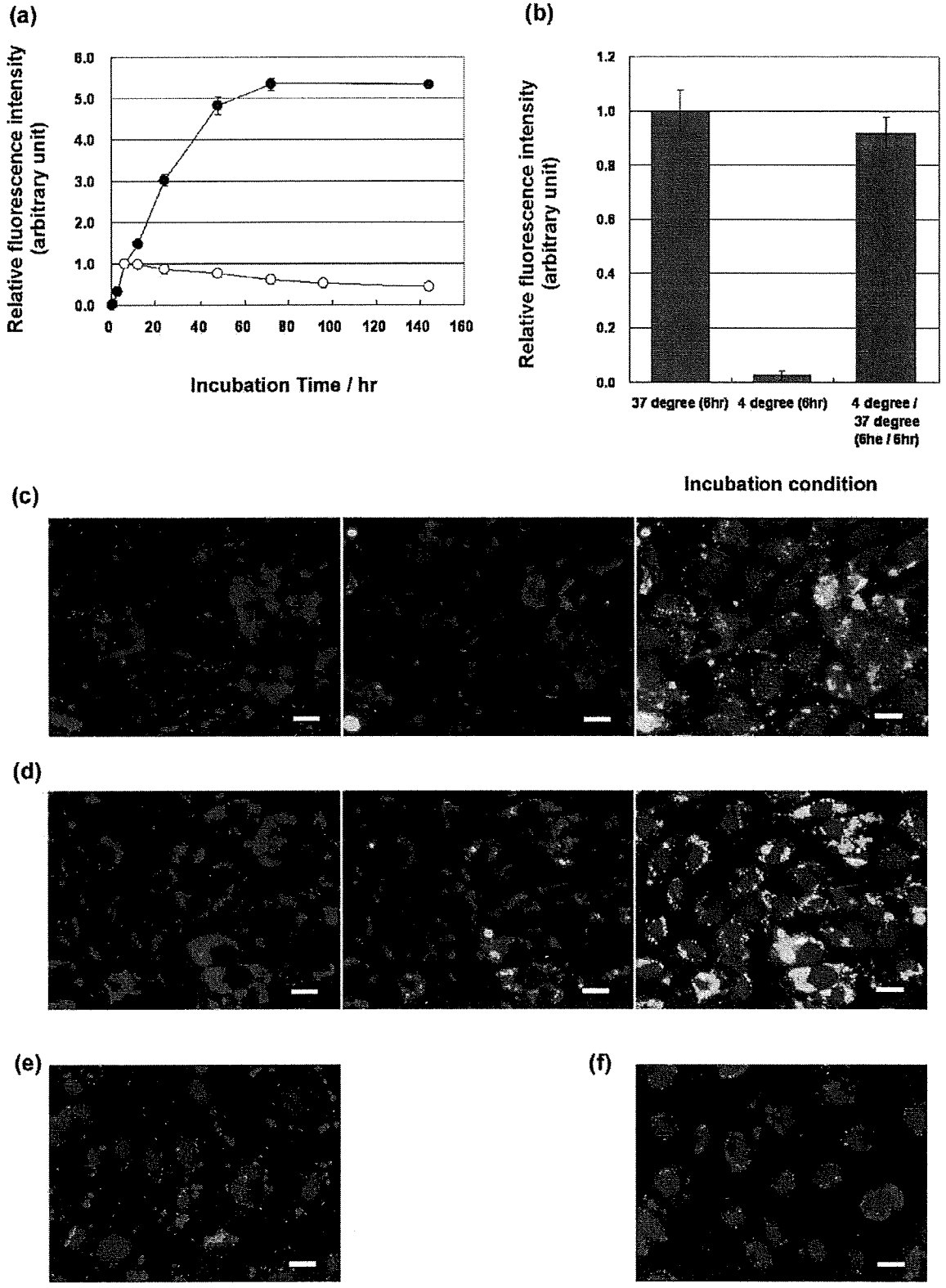

Figure 3. Cellular uptake of fluorescein-labeled amphiphilic polysiloxane (Flu-Am-PAPS). (a) Relative F.I. of Flu-Am-PAPS at each time of incubation with HAECs. The F.I. was measured by integrating brightness at each pixel of fluorescence image and normalized by F.I. at 6 h of incubation. Time course of the cellular uptake of Flu-Am-PAPS by HAECs was represented by closed circles (●). The clearance of the endocytosed Flu-Am-PAPS (○) from HAECs was monitored after HAECs were exposed to the nanoparticles of Flu-Am-PAPS for 6 h and incubated in growth medium. (b) Inhibition and recovery of cellular uptake of Flu-Am-PAPS followed by incubation temperature change (left, 6 h incubation at 37 °C; middle, 6 h incubation at 4 °C; and right, 6 h incubation at 4 °C and then 6 h incubation at 37 °C). Endocytic pathway in HAECs; localization of caveolin-1 and Flu-Am-PAPS in human aortic endothelial cells (HAECs). Caveolin-1 was detected by using primary antibody against caveolin-1 and TRITC-labeled secondary antibody against rabbit. Nucleuses of cells were stained with DAPI. Red: Caveolin-1. Green: Flu-Am-PAPS. Blue: nucleuses. (c) An image taken after 3 h incubation with Flu-Am-PAPS. (d) An image after 24 h incubation with Flu-Am-PAPS. Translocation and accumulation of the nanoparticles of Flu-Am-PAPS were confirmed in HAECs. (e) An image taken after 6 h incubation with Flu-Am-PAPS. (f) An image taken at 18 h of post incubation after the 6 h incubation with Flu-Am-PAPS. Nanoparticles of Flu-Am-PAPS accumulated around the cell nucleus. Scale bar: 20 μm.

platforms for endocytosis and signaling.[21] The caveolae-mediated pathway is prominent and ubiquitous endocytic mechanisms in vascular endothelial cells.[8] Figure 3c and d show fluorescence images of HAECs that incorporated fluorescein-labeled polysiloxane nanoparticles (green) and were immunostained for caveolin-1 (primary antibody against caveolin-1, TRITC-labeled secondary antibody against rabbit; red), which comprises the caveolae. Fluorescence image taken at 3 h of incubation time (Figure 3c) demonstrates that some of the green emissions from nanoparticles (left image in Figure 3c) are overlapped with red emissions from caveolin-1 (middle image in Figure 3c) to make yellow area (right image in Figure 3c). The yellow overlaps suggest that nanoparticles are localized at the caveolae. At 24 h of incubation time, nanoparticles (left image in Figure 3d) were localized as ring-like patterns of overlapped area around nucleuses of HAECs (right image in Figure 3d). This indicates that the nanoparticles of Flu-Am-PAPS were trapped into caveolae in plasma membrane and transported into cytosol of HAECs by 24 h of incubation. The peri-nuclear localization of the nanoparticles (Figure 3f) was also observed when HAECs were exposed to the nanoparticles for 6 h (Figure 3e) and incubated for 18 h after the medium containing nanoparticles was changed to growth medium containing no nanoparticles. The fluorescence imaging data indicate the following process for the uptake of the nanoparticles: (i) the nanoparticles are trapped at caveolae in plasma membrane, (ii) the nanoparticles are internalized into cytosol, and (iii) the nanoparticles are localized at peri-nuclear region. Furthermore, internalization of the nanoparticles into the cytosol of HAECs was confirmed by confocal laser scanning microscopy. The X-Y plane images of HAECs were taken as optical slices with 0.2 μm thick along Z-axis by confocal laser scanning microscope. Figure 4a shows fluorescence intensity profiles of Flu-Am-PAPS along the Z-direction in HAECs. The intensity profiles were obtained by integrating the brightness at each pixel over the whole area of each image, normalizing the intensity to the intensity at basal position ($Z = 0$ μm) and plotting the normalized intensity as a function of depth in a cell. The intenisty maximum was confirmed in each profile (arrow heads in the graph) and indicates the spatio and temporal position of the nanoparticles in HAECs. Although each profile has two maxima at $Z = 0$ μm and at other position in Z-axis respectively, the intensity maximum that we are discusing here is located above the basal level. The position of the intensity maximum shifted gradually from the apical side ($Z = 3$ μm) to the basal side ($Z = 0-1$ μm) of HAECs; $Z = 2.4-2.6$ μm at 1 h, $Z = 1.1-1.9$ μm at 3 h, $Z = 0.5-1.6$ μm at 6 h, and $Z = 0.4-1.2$ μm at 24 h. Thus, the peak shift clearly shows that the nanoparticles were trapped at the plasma membrane and internalized into the cytosol of HAECs.

The nanoparticles of the amphiphilic polysiloxane can fit into caveolae in the plasma membrane of HAECs, because the histogram of the particle size (Figure 2 (a)) for the nanoparticles of Flu-Am-PAPS indicates that at least 48% of the total population of the nanoparticles have diameters in the range of 10−100 nm, that is comparable to the dimension of caveolae (50−100 nm in both opening diameter and depth). Fluorescence microscope observation demonstrated the colocalization of the nanoparticles and caveolae (Figure 3c and d). To specify the endocytic pathway for the uptake of the nanoparticles we attempted to observe caveolae in HAECs by TEM. Specimens for TEM were prepared by the methods described in the materials and methods after HAECs were incubated with nanoparticles of gold nanoparticle labeled Am-PAPS (Au-Am-PAPS) or Flu-Am-PAPS at 37 °C for 3 h. The nanoparticles (Flu-Am-PAPS) uptaken by HAECs were detected by immunolabeling using anti-fluorescein IgG as a primary antibody and a secondary antibody attached to a gold nanoparticle (diameter: 5 nm). Here we observed TEM specimens by following the two different methods: conventional ultrathin section and rapid-freeze deep-etch immunoreplication.[22] The ultrathin section image (Figure 4b) shows that caveolae (round-shape structures with diameters of about 100 nm: indicated by a square in Figure 4b) are incorporated into cytosol and that dark dots (5−10 nm in diameter) of gold nanoparticles attached to polysiloxane are confirmed in the inner perimeter of caveolae vesicles (indicated by arrows in the inset of Figure 4b). Figure 4c shows the ultrathin section image of cytosol of the intact HAECs (not treated with the nanoparticles of Au-Am-PAPS), showing caveolae in cytosol of HAECs. Caveolae in cytosol of HAECs were detected by immunostaining of caveolin-1 using rabbit anti-caveolin-1 IgG and gold nanoparticles (10 nm of diameter) conjugated anti-rabbit IgG. Gold nanoparticles with 10 nm of diameter were specifically accumulated around the outer perimeter of round-shape structures with diameters of about 100 nm (Figure 4c). The result of immunodetection of caveolae indicates that the round shape structures in cytosol of HAECs are caveolae and provides an evidence that nanoparticles of Au-Am-PAPS are trapped in caveolae. Thus, the ultrathin section image of HAECs indicates that the nanoparticles of Au-Am-PAPS are trapped in caveolae at the plasma membrane of HAECs and are internalized into cytosol of HAECs. In addition to the nanoparticles trapped in caveolae, dark spots with a diameter of 5−10 nm (surrounded by circle in Figure 4b) were confirmed in cytosol of HAECs (Figure 4b). These spots are assigned to gold nanoparticles attached to amphiphilic polysiloxane (Au-Am-PAPS). The different localization of polysiloxane nanoparticles in cytosol of HAECs suggests that there are at least two different pathways in the cellular uptake of polysiloxane nanoparticles: caveolae and the other pathways, including clathrin-coated pits and macropinocytosis. Furthermore, we observed the undercoat structure on the cytoplasmic surface of the upper cell membrane using rapid-freeze deep-etch immunoreplication so as to obtain a detailed view of the cellular uptake of the nanoparticles via caveolae as main endocytic pathways for the uptake of polysiloxane nanoparticles. Fine structures of plasma membrane such as filamentous netlike structure of actin filaments, clathrin coated pits, and caveolae can be preserved by rapid freezing at the cooling speed of 10^5 °C/sec in specimen preparation. The extreme cooling speed does not cause any ice nucleation that can damage the organized structure of the membrane skeleton. In a recent study by Morone and Kusumi,[22] they applied the rapid-freeze replication method to the electron microscopy observation of the membrane skeleton and succeeded in viewing the fine structure of the membrane skeleton with nanometer scale resolution and demonstrating that the membrane skeleton mesh corresponds to the membrane compartment model that was suggested by the study of the diffusion of membrane molecules. Figure 4d and e are TEM images of the undercoat structure of the bottom cell membrane of HAECs before and after the exposure to the nanoparticles of Flu-Am-PAPS. The images were taken using a specimen that was processed by the rapid-freeze and deep-etch method. Caveolae (the characteristic striated round structures: 50−100 nm in diameter), clathrin-coated pits (the characteristic basket-like structures: 100−200 nm in diameter), and actin filaments were confirmed in the upper cell membrane of the intact HAECs (Figure 4d). The nanoparticles of Flu-Am-PAPS endocytosed

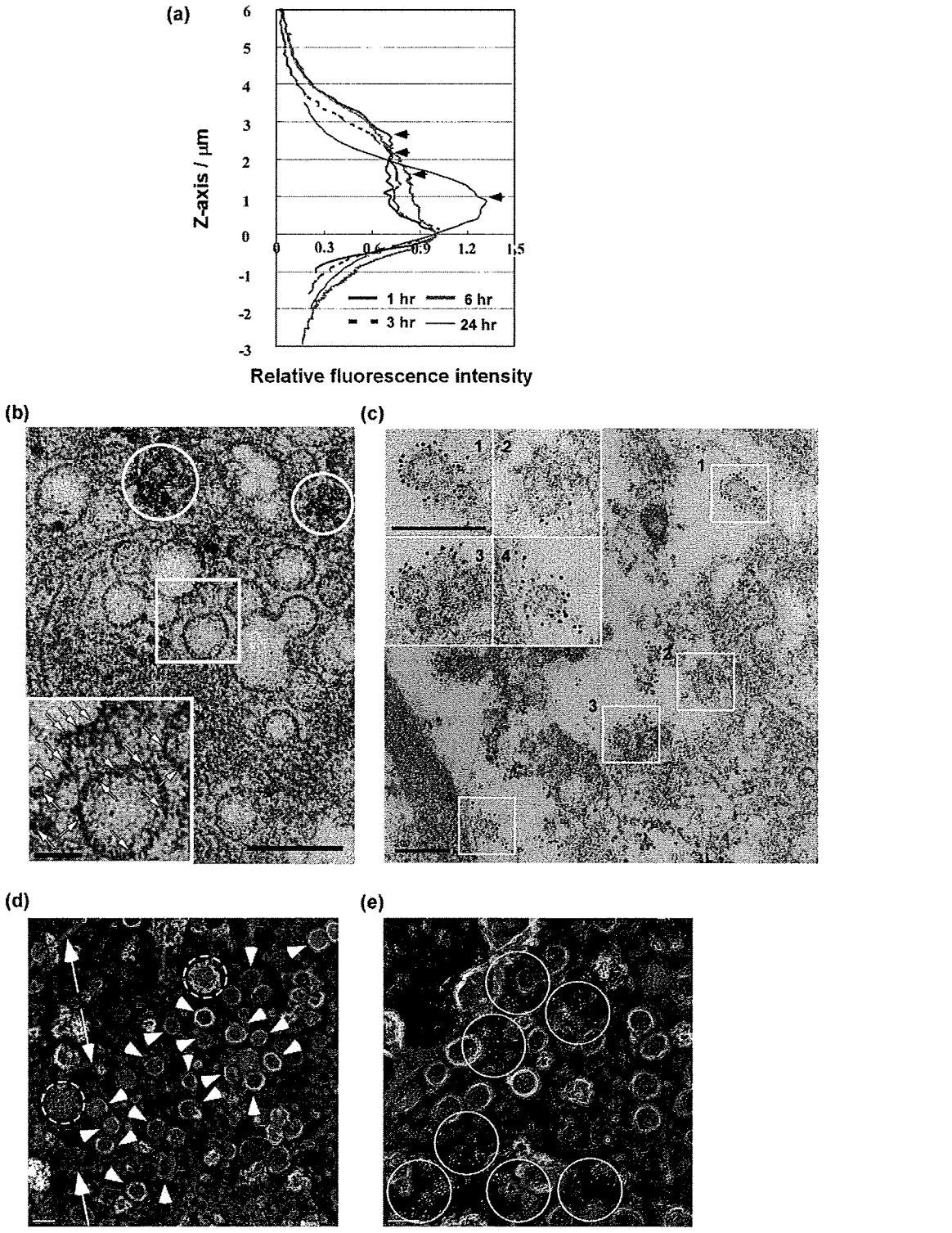

Figure 4. Internalization of nanoparticles of Flu-Am-PAPS in HAECs. (a) F.I. profiles of Flu-Am-PAPS in HAECs. F.I. was calculated by integrating brightness at each pixel over an optical section of confocal fluorescence image. The F.I. is plotted against the *Z*-axis position of each optical section in a confocal fluorescence image. Arrow heads indicates the intensity maximum in the profiles. The intensity maximum can reflect the most probable location of nanoparticles of Flu-Am-PAPS in HAECs at each incubation time. TEM observation of caveolae-mediated endocytosis in HAECs. Ultrathin sections were cut out from embedded HAECs in the direction parallel to the culture dish surface. In the ultrathin section image (b) the nanoparticles of Au-Am-PAPS were incorporated into cytosol of HAECs. Small black dots derived from gold nanoparticles attached to the amphiphilic polysiloxane with diameter of 5−10 nm are confirmed in the inner perimeter of caveolae (indicated by square). The inset is a two-times magnified image of the area indicated by square and shows clearly the small black dots in caveolae (indicated by arrows); (c) immunodetection of caveolae structures in cytosol of HAECs. Caveolae were confirmed by specific accumulation of 10 nm gold nanoparticles of secondary IgG (dark black dots) around the round structures with diameters of 100 nm in cytosol. Scale bars in Figure (b) and (c) represent 200 nm. Scale bars in the insets are 100 nm in (a) and 200 nm in (b). Rapid-freeze, deep-etch immunoreplication TEM images ((d) and (e)) show the undercoat structure of the upper cell membrane enriched in caveolae (indicated by arrow heads), (d), and the gold nanoparticles (white spots in circles) indicating the existence of the Flu-Am-PAPS in the caveolae-enriched area, (e). Other fine structures in (d) are clathrin coated pits (indicated by circle with broken line) and filamentous actin (indicated by arrow). Scale bar: 100 nm.

by HAECs were detected by indirect immunolabeling method with 5 nm diameter colloidal gold particles. Figure 4e shows that the gold particles for immunolabeling of Flu-Am-PAPS that were identified as the dispersed white spots in the TEM image appeared on the internal face of the upper cell membrane and that the gold particles were localized in the area where caveolae were densely accumulated (Figure 4e). The localization of gold particles in cell membrane means that the nanoparticles of Flu-Am-PAPS are localized in the caveolae accumulated area of the upper cell membrane and strongly suggests that caveolae can function as pathways in endocytosis when the nanoparticles of Flu-Am-PAPS are endocytosed into HAECs.

As for the particle size of the endocytosed nanoparticles, we extracted the endocytosed nanoparticles (Flu-Am-PAPS) from HAECs by using a surfactant free protein extraction method and measured the size of the extracted nanoparticles by DLS. According to the histogram of the particle size of the extracted nanoparticles in cytoplasmic fraction of HAECs (the histogram data are attached to Supporting Information as Figure S2), the histogram peak corresponding to the intact nanoparticles of Flu-Am-PAPS (the histogram peak at 150 nm in Figure S2b) shifted to smaller particle size (the histogram peak at 100 nm in Figure S2a) after the endocytosis into HAECs. This suggests that the nanoparticles of Flu-Am-PAPS comparable to the caveolae size are preferentially endocytosed by HAECs. Furthermore, we performed a DLS measurement of the collected sample including serum proteins of growth medium, nanoparticles of Flu-Am-PAPS, and cell debris after the incubation with HAECs and found that the histogram peak of the polysiloxane nanoparticles shifted from 150 nm (before incubation) to 250 nm (the histogram peak in Figure S2c) after the incubation with HAECs. This suggests that the polysiloxane nanoparticles that are larger than the caveolae size are more difficult to be endocytosed and remain after the incubation with HAECs. From the above experiment data of immunofluorescence microscopy, electron microscopy, and particle size measurement, it can be concluded that nanoparticles of amphiphilic polysiloxanes comparable to caveolae size are endocytosed via caveolae in plasma membrane of HAECs.

NO Release in HAECs. NO is a vasodilator synthesized in endothelial cells and plays important physiological roles such as the regulation of blood pressure and the inhibition of platelet adhesion.[7] As we mentioned the endocytic pathways for the uptake of the nanoparticles, caveolae are main routes in endocytosis and gateways to signal-transducing domain where inactive eNOS molecules are localized. It is an intriguing question whether the uptake of the nanoparticles can work in the activation of eNOS, if so, how it does. To study the influence of the nanoparticles on the expression of cell function, nitric oxide release of HAECs was monitored by using diaminorhodamine-4 acetoxymethyl ester (DAR-4 M AM), a fluorescent indicator for NO.[18] DAR-4 M AM can permeate through plasma membrane, be distributed to cytosol, specifically react with NO, and form a fluorescent triazole compound. HAECs were exposed to Dulbecco's modified Eagle medium containing 50 μM DAR-4 M AM for 10 min after the 6 h incubation with nanoparticles of Am-PAPS (0.1 mg/mL). NO release followed by the cellular uptake of polysiloxane nanoparticles could be detected by fluorescence microscope observation of the fluorescence intensity change that results from the triazole compound formation. Figure 5 shows the time profiles of fluorescence intensity of the reaction product derived from NO release after the incubation with nanoparticles (closed triangle), the treatment with bradykinin, endogenous eNOS activator (open circle), the incubation

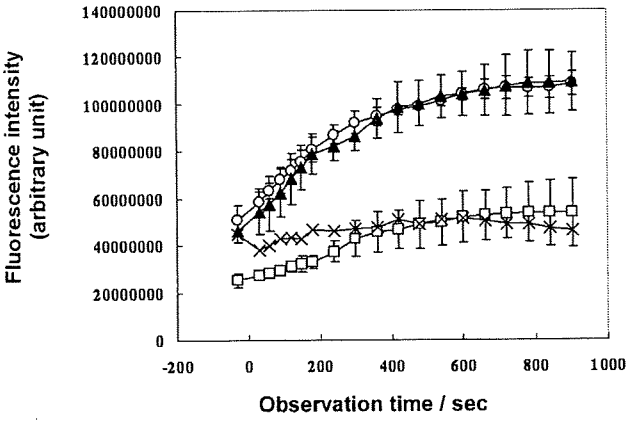

Figure 5. NO release in HAECs. Time profiles of NO release of HAECs. NO was detected by fluorescent indicator, diaminorhodamine-4 acetoxymethyl ester (DAR-4 M AM). The profile represented by open circles shows the NO release after the stimulation with bradykinin (n = 4). The profile represented by closed triangles shows the NO release after the cellular uptake of the nanoparticles of amphiphilic polysiloxane (n = 4). The profile represented by open squares shows the NO release after the cellular uptake of the sugar conjugated water-soluble polysiloxane (n = 3). The NO release profile in resting HAECs was indicated by cross (n = 3). The error bar in each data point is represented by standard deviation.

with water-soluble polysiloxane for positive control (open square), and the incubation in DMEM for negative control (cross symbol). After the uptake of nanoparticles, NO release of HAECs was enhanced up to the same release level that was observed when endothelial cells were stimulated by bradykinin. As a preliminary study about the effect of other nanomaterials on NO release in HAECs, we tested NO release level using commercially available polystyrene nanoparticles, micromer (Micromod, Rostock, Germany) in comparison with that using our polysiloxane nanoparticles. A similar trend in NO release was observed when HAECs were incubated with a growth medium containing 1 mg/mL of the polystyrene nanoparticles with 50 nm of diameter (time profile of NO release represented by open squares of Figure S3 in Supporting Information). However, the polystyrene nanoparticles with 200 nm of diameter did not enhance NO release level (time profile of NO release represented by closed squares of Figure S3 in Supporting Information). This suggests that nanoparticles with caveolae size could enhance NO release in HAECs. Furthermore, NO release followed by 6 h incubation with a nonassociative water-soluble sugar conjugated polysiloxane (Figure 1b; concentration, 1 mg/mL) was less than half of the NO release level induced by the amphiphilic polysiloxane nanoparticles and exhibited a time profile that was quite similar to that without stimulation (negative control: cross symbols in Figure 5). As a result of these data, the enhanced release of NO after the incubation with polysiloxane nanoparticles suggests that signal transduction leading to NO release is activated upon the cellular uptake of the nanoparticles via caveolae.

Activation of Endothelial Nitric Oxide Synthase (eNOS) Coupled to Nanoparticle Uptake. In resting endothelial cells, some of the eNOS molecules are inhibited by protein complex formation with caveolin-1, a constituent protein of caveolae. Cell stimulation with Ca^{2+}-mobilizing agonists such as bradykinin promotes calmodulin binding to eNOS and dissociation of eNOS from caveolin-1. The dissociated eNOS molecules can be detected in intracellular sites close to nucleus.[23] Such a subcellular migration of signaling proteins followed by their activation is known as translocation. The translocation of eNOS

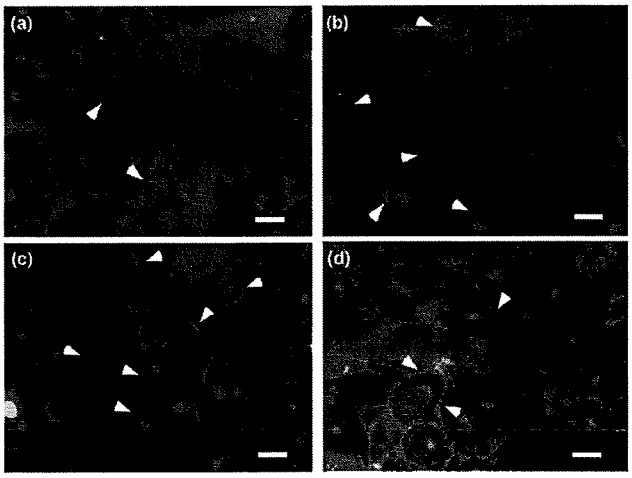

Figure 6. Translocation of eNOS in HAECs in response to bradykinin and upon cellular uptake of the nanoparticles of Am-PAPS. (a) Representative image of eNOS localization in resting HAECs (arrowhead). eNOS was redistributed from the cell periphery to intracellular sites near the nucleus (arrowheads in (b) and (c)) when HAECs were treated with 1 μM bradykinin for 5 min, (b), or were incubated with the nanoparticles of Am-PAPS (0.1 mg/mL) for 6 h, (c). eNOS did not translocate to peri-nuclear region of HAECs when HAECs were exposed to sugar conjugated water-soluble polysiloxane (1 mg/mL) for 6 h, (d). Scale bar in each image is 20 μm.

is followed by the activation of eNOS in endothelial cells.[23] Phosphorylation of eNOS on Ser^{1177} occurs concomitantly in the activation process of eNOS.[24] Here we studied the influence of nanoparticle uptake of HAECs on the eNOS activation with respect to the intracellular translocation and the phosphorylation of eNOS. Immunofluorescence imaging of HAECs using monoclonal antibody to eNOS demonstrated that eNOS bound to cell membrane (cell periphery: Figure 6a) translocate to the cell cytosol and the peri-nuclear region upon 5 min stimulation with 1 μM of bradykinin (Figure 6b). The translocation of eNOS was confirmed as ring-like patterns around nucleuses after the HAECs were exposed to nanoparticles of Am-PAPS for 6 h (Figure 6c). This suggests that caveolae-mediated endocytosis of nanoparticles in HAECs can be coupled to the eNOS activation and can work as an external stimuli in a signal transduction where membrane-bound eNOS are activated. Phosphorylation of eNOS at Ser^{1177} (P-eNOS) was detected by Western blot analysis. Figure 7a shows that phosphorylation of eNOS occurred when HAECs were incubated with the nanoparticles of Am-PAPS. The target proteins (eNOS and P-eNOS) transferred to PVDF membranes were detected by colorimetric reaction of TMB substrate. The protein levels of the target proteins were evaluated by measuring the intensity of the reaction product stained on the blotted bands. In Figure 7b the target protein levels were plotted against time of the incubation with nanoparticles. The total amount of eNOS gradually decreased to 65% of the initial amount of eNOS at 6 h of incubation while HAECs were incubated with polysiloxane nanoparticles (the time profile of eNOS: closed squares in Figure 7b). β-Tubulin, a loading control for Western blot analysis, exhibited a slight decrease in expression level during the incubation with polysiloxane nanoparticles (the time profile of β-tubulin: closed circles in Figure 7b), although the same amount of extracted proteins (2 μg) was applied to each lane in SDS-PAGE. This indicates that incubation with polysiloxane nanoparticles influences the expression level of eNOS in HAECs. On the other hand, the P-eNOS (Ser^{1177}) level gradually increased by 1.3 fold at 1 h of incubation and by 1.6-fold at

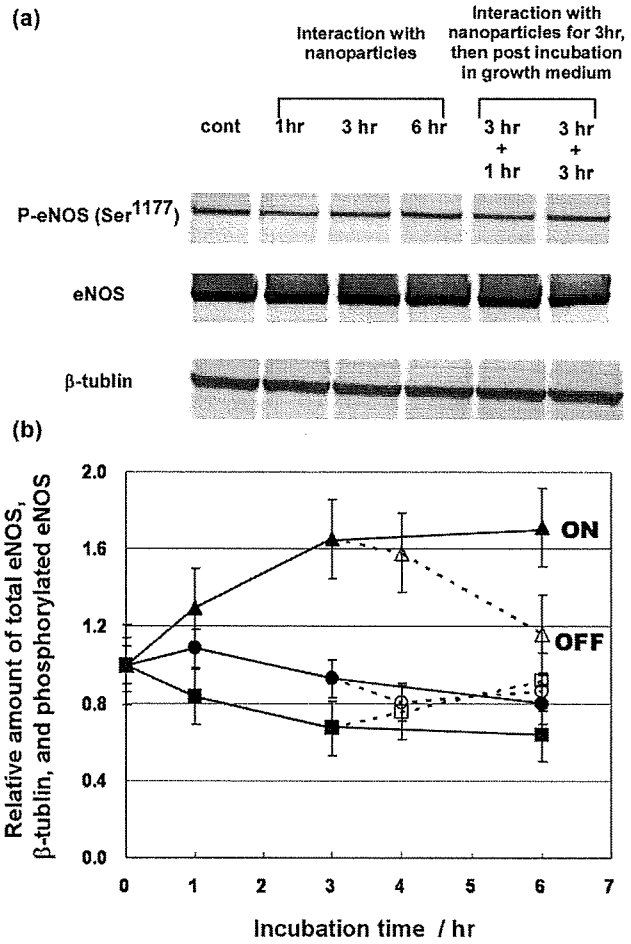

Figure 7. Nanoparticles of amphiphilic polysiloxane (Am-PAPS) stimulate phosphorylation of eNOS. HAECs were incubated with nanoparticles of Am-PAPS for the time period indicated. (a) Cell lysates were analyzed by Western blot with antibodies for phosphorylated eNOS-Ser1177, eNOS, and β-tubulin. (b) The bands of target proteins were quantified by measuring the colorimetric intensity. The graph shows the time course of the expression level of the target proteins (▲, △: P-eNOS, ■, □: e-NOS, and ●, ○: β-tubulin). The time courses represented by closed symbols demonstrate the expression level of the proteins of interest during the incubation with polysiloxane nanoparticles. The time course of the proteins of interest after the removal of polysiloxane nanoparticles at 3 h of incubation are depicted by open symbols and dotted lines. Each data point represents the means ± SE (n = 3).

3 h from the initial phosphorylation level of eNOS (the time profile of P-eNOS: closed triangles in Figure 7b). The expression level of P-eNOS reached saturation point at 6 h of incubation with polysiloxane nanoparticles. Thus, the activation of eNOS was followed by the cellular uptake of polysiloxane nanoparticles and the expression level of P-eNOS was maintained as long as HAECs were exposed to the nanoparticles. Furthermore, the expression levels of target proteins (eNOS, P-eNOS, and β-tubulin) were back to the initial level of each protein (time profiles (from 3 to 6 h of incubation time) indicated by open symbols and dotted lines in Figure 7b) when polysiloxane nanoparticles were removed from culture medium and HAECs were incubated in a fresh growth medium for 3 h after the removal of nanoparticles. These data suggest that phosphorylation of eNOS at Ser^{1177} is stimulated by interaction with nanoparticles and the enhanced level of phosphorylation is maintained transiently during the interaction with polysiloxane nanoparticles. Meanwhile, any eNOS translocation was not

observed at all when HAECs were exposed to the water-soluble sugar conjugated polysiloxane (concentration: 1 mg/mL) for 24 h (Figure 6d). According to the result of fluorescence image analysis for the estimation of the amount of the endocytosed polymers, the amount of the incorporated water-soluble polysiloxane at 24 h of the incubation was approximately 15% of that of the incorporated fluorescein-labeled nanoparticles (Flu-Am-PAPS) at 6 h of the incubation time (Figure S4 is available at Supporting Information). The water-soluble polysiloxane was certainly endocytosed by HAECs; however, the eNOS activation did not occur. These results suggest that the types of the polymers (nonassociative polymer chains or nanoparticles of amphiphilic polymers) exposed to cells and the pathways (caveolae or clathrin coated pits) selected in endocytosis are important factors that can influence the signal transduction in the regulation of cell function. Thus, we assume that the delivery of the nanoparticles targeted to caveolae facilitates eNOS activation (subcellular translocation and phosphorylation at Ser^{1177}) and the activated eNOS promotes NO release. The details of the mechanism underlying the eNOS activation upon the caveolae-mediated endocytosis of our polysiloxane nanoparticles is still under investigation and will be reported elsewhere.

Conclusion

In conclusion, the nanoparticles of amphiphilic polysiloxane were endocytosed via caveolae in human aortic endothelial cells and the uptake of the nanoparticles promoted nitric oxide release in HAECs. Caveolae is a membrane microdomain where various signal transduction molecules are accumulated and external stimuli are processed. Endothelial nitric oxide synthase is one of the constituent molecules in signal transduction and plays a significant role in regulation of vasorelaxation by synthesizing nitric oxide. Some of eNOS molecules are bound to caveolin-1 and deactivated in caveolae. Activation of eNOS is triggered in vivo by binding of physiological active molecules such as bradykinin, angiotensin-II, and estrogen to their corresponding receptors in endothelial cells. According to the recent study by Maniatis et al., eNOS-dependent NO production is coupled to caveolae-mediated endocytosis induced by albumin binding protein gp60 (albumin receptor).[25] In their case, NO release started just after gp60 activation by adding BSA and lasted up to 20 min. Phosphorylation of eNOS accompanied by gp60 activation was confirmed at just 30 s after the addition of BSA. This means that BSA uptake via caveolae in rat lung microvascular endothelial cells is quickly processed as an external signal and leads to NO release. In our study, a delay of 15−60 min between the beginning of the nanoparticle uptake and the onset of the induced phosphorylation of eNOS was observed. This kind of delay was rather observed in the phosphorylation of eNOS that was stimulated by shear stress to bovine aortic endothelial cells.[26] Sustained phosphorylation of eNOS is another feature of eNOS activation that is followed by nanoparticle uptake of HAECs. We found that the phosphorylation of eNOS lasted while HAECs were exposed to nanoparticles for 6 h. The phosphorylation of eNOS induced by gp60 activation lasted at most for 30 min. Furthermore, there was considerable difference in the working concentration of stimulants for the activation of eNOS between BSA (5 mg/mL) and our nanoparticles (0.1 mg/mL or less). We think that there are some different mechanisms in the activation of eNOS induced by caveolae-mediated endocytosis between former study using BSA and our current study using artificial nanoparticles. In any case, nanoparticle uptake by HAECs stimulates the activation of eNOS and raises the NO production. This means that nanoparticles can be regarded as extracellular signals. Concerning the influence of the interaction between nanomaterials with cells on the expression of cell function, a study on the behavior of bovine carotid arterial endothelial cells cultured on polyurethane nanocomposites demonstrated that cell migration could be regulated by the surface morphological change induced by blending gold nanoparticles with polyurethane and revealed that the promoted migration was associated with up-regulation of eNOS expression via the activation of PI3K/Akt signaling pathway.[27] The key phenomena explaining the promoted cell migration is signal transduction associated with the interaction between cells and the nanostructured surface and concomitant rearrangement of cytoskeleton. Meanwhile, our study deals with signal transduction associated with endocytosis of nanoparticles that are targeted to membrane microdomains of cells. As far as we know, this is the first demonstration that nitric oxide release in HAECs can be induced by the caveolae-mediated cellular uptake of artificial nano materials of synthetic polymer and that the uptake itself can work as external stimuli leading to the expression of a cell function. Thus, nanoparticle can work as an artificial signal substance whose signaling characteristics may be tuned by molecular design of constituting amphiphilic polymers as well as the nanoparticles can be used as nanocarriers in drug delivery system. In the drug delivery system the nanocarrier itself should be inert to targeted cells and tissues. However, as we demonstrated in this study, nanoparticles can influence cell functions; nanoparticles may not only promote the pharmacological effects of delivered drugs but also cause undesirable effects in the target tissues or cells. The molecular design of constituent molecules for nanoparticles and the interaction between nanoparticles and cells should be considered more carefully in terms of the activation of cell functions. Nevertheless, we expect that targeting delivery of nanoparticles including our polysiloxane nanoparticles to caveolae is a potential and novel medication to hypertension based on the regulation of NO release by switching of eNOS activation in a single cell.

Acknowledgment. T.N. thanks Professor Mitsuru Akashi and Dr. Takami Akagi of Osaka University for allocating instrument time of dynamic light scattering measurement, Dr. Tetsuji Yamaoka and Dr. Atsushi Mahara of National Cardiovascular Center Research Institute for allocating instrument time of fluorescence spectroscopy measurement, Dr. Tsutomu Furuzono of National Cardiovascular Center Research Institute for allocating instrument time of microplate reader in protein assay, and Mrs. Mina Kaneko for technical work in cell culture experiments. Part of this research was financially supported by Terumo Life Science Foundation in fiscal year of 2008.

Supporting Information Available. Supplementary data of nanoparticle size change in physiological condition, size of nanoparticles endocytosed, and cellular uptake of water-soluble polysiloxane. This material is available free of charge via the Internet at http://pubs.acs.org.

References and Notes

(1) Simons, K.; Ikonen, E. *Nature* **1997**, *387*, 569–572.
(2) Minshall, R. D.; Sessa, W. C.; Stan, R. V.; Anderson, R. G. W.; Malik, A. B. *Am. J. Physiol.* **2003**, *285*, L1179–L1183.
(3) Gratton, J.-P.; Bernatchez, P.; Sessa, W. C. *Circ. Res.* **2004**, *94*, 1408–1417.
(4) Wyatt, A. W.; Steinert, J. R.; Mann, G. E. *Biochem. Soc. Symp.* **2004**, *71*, 143–156.

(5) Vallance, P.; Chan, N. *Heart* **2001**, *85*, 342–350.
(6) McIntosh, D. P.; Tan, X.-Y.; Oh, P.; Schnitzer, J. E. *Proc. Natl. Acad. Sci. U.S.A.* **2002**, *99*, 1996–2001.
(7) Michel, T. *Braz. J. Med. Biol. Res.* **1999**, *32*, 1361–1366.
(8) Muro, S.; Koval, M.; Muzykantov, V. *Curr. Vasc. Pharmacol.* **2004**, *2*, 281–299.
(9) Sanvicens, N.; Marco, M. P. *Trends Biotechnol.* **2008**, *26*, 425–433.
(10) Conner, S.; Scmid, S. L. *Nature* **2003**, *422*, 37–44.
(11) Cruz, T.; Gaspar, R.; Donato, A.; Lopes, C. *Pharm. Res.* **1997**, *14*, 73–79.
(12) Mark, J. E.; Allcock, H. R.; West, R. In *Inorganic Polymers*, 2nd ed.; Oxford University Press: New York, 2005; pp 154−199.
(13) Kichler, A.; Sabourault, N.; Décor, R.; Leborgne, C.; Schmutz, M.; Valleix, A.; Danos, O.; Wagner, A.; Mioskowski, C. *J. Controlled Release* **2003**, *93*, 403–414.
(14) Moghimi, S. M.; Hunter, A. C.; Murray, J. C. *Pharmacol. Rev.* **2001**, *53*, 283–318.
(15) Beppu, K.; Kaneko, Y.; Kadokawa, J.; Mori, H.; Nishikawa, T. *Polym. J.* **2007**, *39*, 1065–1070.
(16) Tominaga, H.; Ishiyama, M.; Ohseto, F.; Sasamoto, K.; Hamamoto, T.; Suzuki, K.; Watanabe, M. *Anal. Commun.* **1999**, *36*, 47–50.
(17) Heuser, J. *Traffic* **2000**, *1*, 545–552.
(18) Kojima, H.; Hirotani, M.; Nakatsubo, N.; Kikuchi, K.; Urano, Y.; Higuchi, T.; Hirata, Y.; Nagano, T. *Anal. Chem.* **2001**, *73*, 1967–1973.
(19) Kaneko, Y.; Iyi, N.; Kurashima, K.; Matsumoto, T.; Fujita, T.; Kitamura, K. *Chem. Mater.* **2004**, *16*, 3417–3423.
(20) Durin, G.; Cottin, S.; Blanc, E.; Rees, A. R.; Temsamani, J. *J. Biol. Chem.* **2003**, *278*, 31192–31201.
(21) Drab, M.; Verkade, P.; Elger, M.; Kasper, M.; Lohn, M.; Lauterbach, B.; Menne, J.; Lindschau, C.; Mende, F.; Luft, F. C.; Schedl, A.; Haller, H.; Kurzchalia, T. V. *Science* **2001**, *293*, 2449–2452.
(22) Morone, N.; Fujiwara, T.; Murase, K.; Kasai, R.; Ike, H.; Yuasa, S.; Usukura, J.; Kusumi, A. *J. Cell Biol.* **2006**, *174*, 851–862.
(23) Prabhakar, P.; Thatte, H. S.; Goetz, R. M.; Cho, M. R.; Golan, D. E.; Michel, T. *J. Biol. Chem.* **1998**, *273*, 27383–27388.
(24) Fleming, I.; Busse, R. *Am. J. Physiol.* **2003**, *284*, R1–R12.
(25) Maniatis, N.; Brovkovych, V.; Allen, S. E.; John, T. A.; Shajahan, A. N.; Tiruppathi, C.; Vogel, S. M.; Skidgel, R. A.; Malik, A. B.; Minshall, R. D. *Circ. Res.* **2006**, *99*, 870–877.
(26) Boo, Y. C.; Sorescu, G.; Boyd, N.; Shiojima, I.; Walsh, K.; Du, J.; Jo, H. *J. Biol. Chem.* **2002**, *277*, 3388–3396.
(27) Hung, H. S.; Wu, C. C.; Chien, S.; Hsu, S. H. *Biomaterials* **2009**, *30*, 1502–1511.

BM900128X

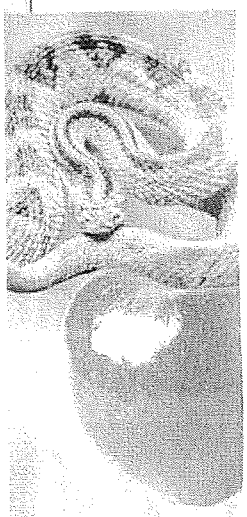

特集 膜蛋白質のシェディングとその制御機構を探る

ADAMファミリー蛋白質の立体構造と作用機構

Three-dimensional domain architecture of the ADAM family proteinases

武田壮一

ADAMファミリー蛋白質は，メタロプロテアーゼドメインと蛇毒ディスインテグリン様のDドメインをもち，蛋白質分解と細胞-細胞間の結合という異なる2つの機能をもつ蛋白質として注目されてきた．しかし，X線結晶解析の結果から，ADAMファミリー蛋白質のDドメインは，当初の想定と異なり，インテグリンとの相互作用には適した構造をもたないことが判明した．一方で，Dドメインの下流のシステイン残基に富む領域は，新規のフォールドをもつ蛋白質間相互作用モチーフであることが判明した．ここでは，ADAMファミリー蛋白質について，最近の構造生物学的な知見を紹介する．

Key words ●メタロプロテアーゼ ●ディスインテグリン ●蛋白質間相互作用 ●X線結晶構造解析

はじめに

1992年，受精における膜融合にかかわる精子表面蛋白質として報告されたファーティリン（Fertilin）は，出血蛇毒に由来する血小板凝集阻害蛋白質ディスインテグリンと非常に似た配列（以降，Dドメインとよぶ）と，ウイルスの融合ペプチド様の配列，および，膜貫通領域をもち，膜融合やインテグリンを介した細胞間相互作用（ここでは，精子-卵相互作用）の新しい担い手となる蛋白質として注目された[1]．ファーティリンの膜融合への関与はいまだ明確ではないが，前駆体がDドメインの上流に蛇毒メタロプロテアーゼ様の配列（以降，Mドメインとよぶ）をもつことがわかり，そののち，ファーティリンと同様に，MドメインとDドメインとを含む遺伝子産物がつぎつぎとみつかる発端となった．これら一群の蛋白質は，2つの特徴的な機能ドメインをもつことと蛋白質の由来から，ADAM（a disintegrin and metalloproteinase）ファミリー蛋白質と命名された[2,3]．

1997年，TNFαのエクトドメインシェディング（ectodomain shedding，以下，単にシェディングとよぶ）にかかわる酵素TACE（TNFα converting enzyme，TNFα変換酵素）が17番目のADAMファミリー蛋白質ADAM17として報告され，ADAMファミリー蛋白質が細胞表層蛋白質のシェディング酵素として注目されるようになった[4,5]．シェディング酵素としてのADAMファミリー蛋白質の役割については，本特集の他項を参照されたい．ADAMファミリー蛋白質は多様な細胞表層蛋白質の切断を行なうが，これらの切断部位の周辺に共通した認識配列はみられず，どのように標的を認識しているかは不明である．また，20個あるヒトADAMファミリー遺伝子のうち，12個は触媒部位のZn^{2+}結合コンセンサス配列（後述）をもつが，ほかはこの配列に変異があり，プロテアーゼ活性の消失しているものと考えられる．前述のファーティリン（Fertilinβ，ADAM2）もそのひとつである．

シェディング酵素として注目される一方で，酵素活性を消失したADAMファミリー蛋白質がどのように機能しているかについてはほとんど理解が進んでいない．Dドメインについては，インテグリンとの相互作用を示唆する結果が多数，報告されている．また，Dドメインの下流にはシステイン残基に富む領域（システインリッチドメイン，以降，Cドメインとよぶ）があり，基質の認識や蛋白質間相互作用にかかわるという報告がなされているが，これらドメインとほかの蛋白質との具体的な相互作用の様式はほとんどわかっていない．組換え蛋白質の大量発現がむずかしいためにADAMファミリー蛋白質に関する構造生物学的な研究は立ち遅れていたが，筆者らは，蛇毒に含まれるADAMファミリーホモログ蛋白質に着目してX線結晶構造解析を進めてきた．本稿では，これらの結晶構造などから明らかにな

Soichi Takeda
国立循環器病センター研究所 心臓生理部
E-mail：stakeda@ri.ncvc.go.jp
URL：http://www.ncvc.go.jp/res/shinzo/shinzoj_01.html

ってきた，ADAMファミリー蛋白質の立体構造とその機能について紹介したい．

I ADAMファミリー蛋白質のドメイン構造

ADAMファミリー蛋白質はN末端側から，シグナル配列，プロペプチド配列につづいて，前述のMドメイン，Dドメイン，Cドメインをもち，その下流に約60アミノ酸残基からなるEGF様ドメインと膜貫通領域をもつ，I型膜貫通蛋白質である[2,6]（図1）．ADAM10およびADAM17はほかのADAMファミリー蛋白質と異なり，EGF様ドメインをもたずCドメインのすぐ下流が膜貫通領域となる．細胞外領域はADAMファミリー蛋白質のあいだで比較的アミノ酸配列の保存性が高いのに対し，細胞内領域は長さ，配列ともに非常に多様である．アダプター蛋白質との結合に関与するSH3ドメイン結合配列やリン酸化部位が存在し，細胞内から細胞外へのシグナル伝達に関与しているものと考えられるが，その作用機序はほとんどわかっていない．膜型ADAMファミリー蛋白質以外に，スプライスバリアントとしてMドメイン，Dドメイン，Cドメインを含む遊離型ADAMファミリー蛋白質も発現しているが，その生理的な役割はよくわかっていない．

1．蛇毒ADAMファミリーホモログ蛋白質

ガラガラヘビ，ハブやマムシなどクサリヘビ科の蛇毒は，さまざまな分子量の蛇毒メタロプロテアーゼ（snake venom metalloproteinase；SVMP）を，種によっては総蛋白質の30％以上も含む．これらはおもに獲物の体内で血管壁を破壊する出血因子としてはたらき，また，血液凝固因子や血小板膜糖蛋白質などにも作用することが知られている[7]．膜型ADAMファミリー蛋白質と異なり，みつかっているすべての蛇毒メタロプロテアーゼはプロテアーゼ活性をもっているものと考えられる．蛇毒メタロプロテアーゼはドメイン構成により，Mドメインのみをもつ P-I型から，後述のRVV-Xに代表されるヘテロ3量体のP-Ⅳ型にまで，分類されている（図1）．研究材料としての蛇毒の有用性は，本誌2009年6月号にて，山崎・森田により紹介されているが[8]，ADAMファミリー蛋白質の研究においても蛇毒が一役買っている．北米生息のニシダイヤガラガラヘビ（*Crotalus atrox*）由来のホモ2量体P-Ⅲ型蛇毒メタロプロテアーゼのVAP1（vascular apoptosis-inducing protein-1），および，

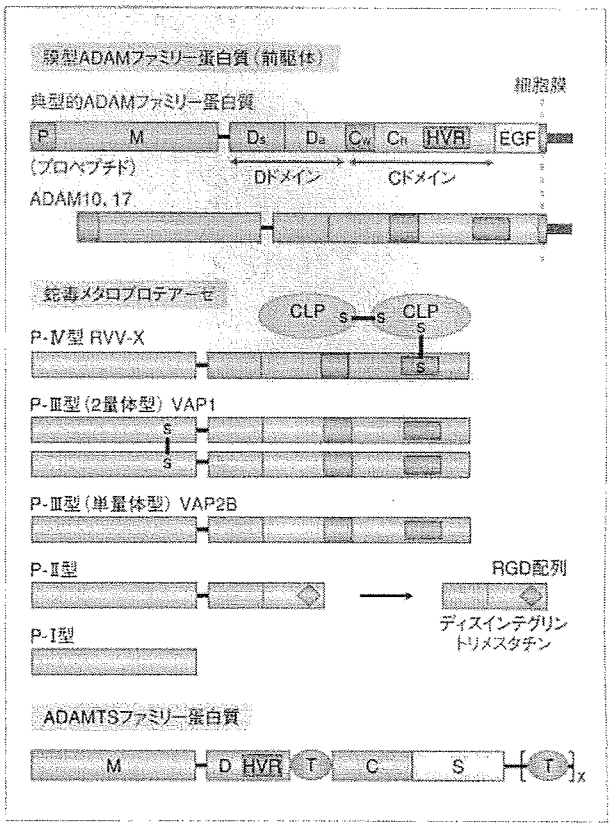

図1 ADAMファミリー蛋白質のドメイン構造

ADAM10およびADAM17以外のすべての膜型ADAMファミリー蛋白質は，Mドメイン，Dドメイン，Cドメインと膜貫通領域とのあいだにEGF様ドメインをもつ．P-Ⅱ型蛇毒メタロプロテアーゼはおもにトランスゴルジネットワークでプロセシングされディスインテグリンとなる[7]．P-Ⅳ型蛇毒メタロプロテアーゼはジスルフィド結合した2本のC型レクチン様サブユニット（CLP）の軽鎖をもつ．
HVR：超可変領域．

単量体P-Ⅲ型蛇毒メタロプロテアーゼのVAP2Bは，連続したMドメイン，Dドメイン，Cドメインの立体構造が最初に決定された蛇毒ADAMファミリーホモログ蛋白質である．これら蛇毒メタロプロテアーゼはヒトADAMファミリー蛋白質の細胞外ドメインとおよそ40％のアミノ酸の同一性を示し，また，立体構造の基本骨格を形成するアミノ酸残基（ジスルフィド結合や後述のCa^{2+}結合にかかわるアミノ酸残基など）は，ほぼすべて保存されている[6,9,10]．

2．Mドメイン，Dドメイン，Cドメイン

P-Ⅲ型蛇毒メタロプロテアーゼのX線結晶構造解析から，膜型ADAMファミリー蛋白質のMドメイン，Dドメイン，Cドメインの立体構造とその構築原理が明らかになった[6,9,10]．この3つのドメインは全体としてC字型の構造

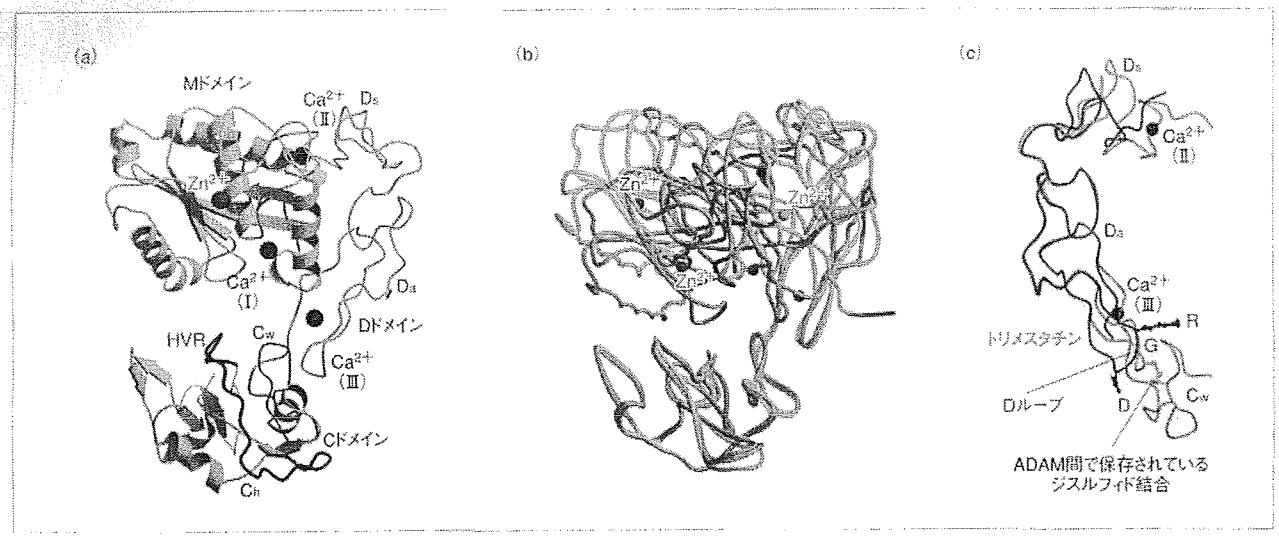

図2　Mドメイン，Dドメイン，Cドメインの立体構造

(a) VAP2Bの結晶構造．ADAMファミリー蛋白質のMドメイン，Dドメイン，Cドメインは全体としてC字型の構造をなし，Zn^{2+}の結合した触媒部位がCドメイン内の超可変領域（HVR）と対面する．Mドメイン，Dドメイン，Cドメインには3箇所（I～III）のCa^{2+}結合部位が存在する．

(b) Mドメイン，Dドメイン，Cドメインの内部の可動性．VAP1（青色），VAP2B（黄色），およびRVV-X（ピンク色）のC_hサブドメインでの重ね合わせ．それぞれに結合したZn^{2+}を，青色，緑色，赤色で示す．C_hサブドメインに対するMドメインの相対位置の違いは，蛋白質の違いというよりはむしろ結晶のパッキングの差に由来し，サブドメインのあいだに可動部のあることがわかった．

(c) VAP2BのD_sサブドメイン/D_aサブドメイン/C_wサブドメインとトリメスタチンとの重ね合わせ．ディスインテグリンにおいてRGD配列を含むDループ（青色で示す）はフレキシブルな構造をもちインテグリン頭部と結合するが，ADAMファミリー蛋白質ではつづくC_wサブドメインとジスルフィド結合を含む連続構造を形成するため，インテグリンとの結合にはかかわらないものと考えられた．

をもっていた（図2a）．約200アミノ酸残基からなるMドメインは5本のαヘリックスと5本のストランドからなるβシートの骨格をもち，さきに構造決定されたP-I型蛇毒メタロプロテアーゼやヒトADAM33のMドメインのみの構造と非常に高い類似性を示した．コンセンサス配列（HEXXHXXGXXHD）の3つのヒスチジン残基にZn^{2+}が配位し，グルタミン酸残基が活性基として機能していた．この触媒部位のちょうど正反対の位置にDドメインとの境界があった．Dドメインはつづくシステインと連続した構造をとり，この2つのドメイン全体としてMドメイン側に湾曲した構造をもつため，Cドメインの末端の部分はMドメインの触媒部位に近い位置にあった．DドメインおよびCドメインはそれぞれサブドメインに分けられ，D_s（ショルダー），D_a（アーム），および，C_w（リスト），C_h（ハンド）と名づけられた．D_sサブドメインおよびD_aサブドメインはほとんど2次構造のない連続したヘアピンループからなっていたが，それぞれ3つのジスルフィド結合にくわえ，Ca^{2+}をコアにもつ強固な構造を形成していた．複数の結晶構造の比較から，各サブドメインのあいだには，程度の差はあれ，可動性のあることがわかった（図2b）．

3．Dループ

ディスインテグリンは蛇毒から単離された血小板凝集阻害因子の総称で，49～84アミノ酸残基からなるポリペプチドであり，多くはP-II型蛇毒メタロプロテアーゼから翻訳後プロセシングにより生じるものと考えられている[7]（図1）．その構造は4～7個のジスルフィド結合により保持され，末端に突出したディスインテグリンループ（Dループ）を提示する．この部分にRGD配列をもつものは，血小板膜のフィブリノーゲン/フォンビルブランド因子受容体であるインテグリン$\alpha_{IIb}\beta_3$の頭部の2つのサブユニットのあいだに形成される溝に拮抗的に結合し，血小板凝集を阻害する[11,12]，また，$\alpha_{IIb}\beta_3$以外のインテグリンにも結合し，それらを発現する細胞と接着因子との結合を拮抗して阻害することが知られている．

ADAMファミリー蛋白質のD_aサブドメインは，RGD配列をもつディスインテグリン，トリメスタチン[11]と非常に類似した構造をもつ（図2c）．しかし，ADAMファミリー蛋白質のDループは例外的なヒトADAM15を除いてRGD配列をもたず，結晶構造ではつづくC_wサブドメインとの境界面を形成し，その中心のジスルフィド結合によりD_aサブ

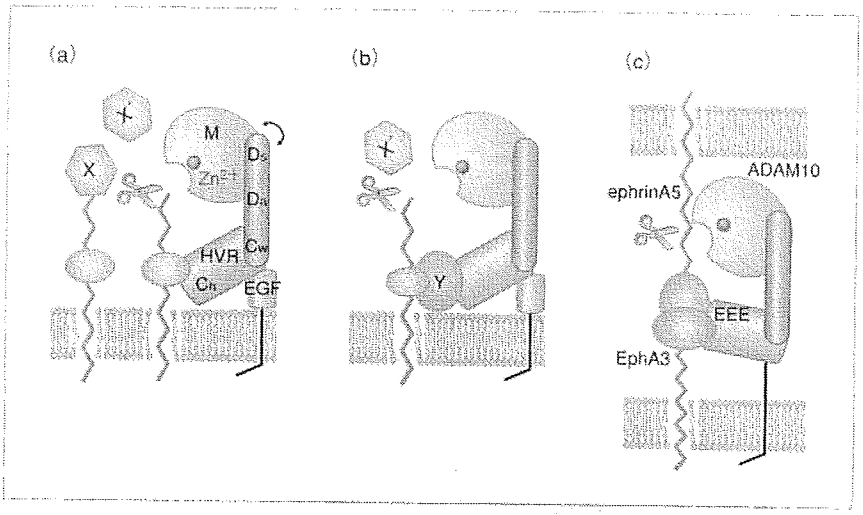

図3 膜型ADAMファミリー蛋白質による基質切断のモデル

(a) 基質蛋白質Xが超可変領域(HVR)により直接に認識され切断されるモデル.
(b) 基質蛋白質Xが結合蛋白質Yを介して超可変領域により間接的に認識され切断されるモデル.
(c) Jonesらによって提案された,ADAM10によるephrinA5切断機構のモデル[13].受容体型チロシンキナーゼEphA3は,隣接する細胞に発現する膜型リガンドであるephrinA5に結合する.ADAM10は,C_hサブドメインにある3つのグルタミン酸残基からなる負電荷クラスター(EEEで示す)でEphA3-ephrinA5複合体を認識し,ephrinA5を*trans*に切断する.ADAM10ではC_wサブドメインとC_hサブドメインとの相対位置がP-Ⅲ型蛇毒メタロプロテアーゼと異なり,超可変領域ではなく負電荷クラスターが触媒部位の方向を向くことが想定された.

ドメインとC_wサブドメインは一体として機能することがわかった[9,10](図2c).同様なD_aサブドメインとC_wサブドメインとの一体構造は,ウシADAM10のDドメイン,Cドメインの結晶構造からも明らかになっている[13].さらに,ADAM10およびADAM17以外のすべてのADAMファミリー蛋白質において,P-Ⅲ型蛇毒メタロプロテアーゼと同様に,Dループ部位はCa^{2+}結合によるしっかりとした裏打ち構造が形成されているものと考えられる[6,9].この点は,ディスインテグリンのDループが誘導適合による蛋白質間相互作用に適した比較的フレキシブルな構造をもつのと対照的である.

これまで,Dループ部の短い合成ペプチドや大腸菌組換え蛋白質で調製したDドメインを用いてインテグリンとの相互作用があるとした結果が数多く報告されているが,多数のジスルフィド結合やCa^{2+}結合をもつADAMファミリー蛋白質のDドメインの機能が正確に検証されているとはいいがたい.結晶構造解析の結果は,ADAMファミリー蛋白質のDループは従来型のインテグリンリガンドとして機能する可能性が非常に低いことを示唆していた.

4. 超可変領域

ADAMファミリー蛋白質のC_hサブドメインにはアミノ酸配列だけでなく立体構造からも既知の構造モチーフとの類似性は見いだせず,新規のフォールドであることがわかった[9,13].Dループ部位がインテグリンとの相互作用に適した構造をもたない一方,C_hサブドメインはC字型のMドメイン,Dドメイン,Cドメインの構造のなかで触媒部位と対面する位置関係にあり,基質認識への関与が示唆された.とくに,触媒部位と対面するC_hサブドメインの末端ループ部位は,ADAMファミリー蛋白質のあいだでもっともアミノ酸配列が可変で長さも多様な領域と一致し,筆者らは,これを超可変領域(hyper-variable region;HVR)と名づけた[9].

興味深いことに,解析したすべてのP-Ⅲ型蛇毒メタロプロテアーゼの結晶において,超可変領域はとなりの蛋白質分子とのパッキングにかかわっており,また,その構造は誘導適合により形成され,逆に,溶液中では超可変領域はフレキシブルな構造をもつものと考えられた.筆者らは,蛋白質内での立体配置や蛋白質間相互作用に適した構造的な特徴から,超可変領域が基質を直接あるいは間接的に結合・認識するエキソサイトである可能性を提案した(図3).ADAM10のDドメイン,Cドメインの結晶構造においては,C_wサブドメインとC_hサブドメインとのあいだの向きがP-Ⅲ型蛇毒メタロプロテアーゼとは異なり,その結果,ADAM10の超可変領域は触媒部位とは対面しないものと考えられた[9,13].しかし,その一方で,触媒部位の側に向くと考えられる3つのグルタミン酸残基からなる負電荷クラスターが,EphA3-ephrinA5複合体を認識しephrinA5を*trans*に切断するのに関与すると報告されている[13](図3c).

超可変領域が基質認識のエキソサイトであるという仮説は膜型ADAMファミリー蛋白質においていまだ検証されていないが,ADAMファミリー蛋白質と類縁のADAMTS(ADAM with thrombospondin motif)ファミリー蛋白質の部分結晶構造から,非常に興味深いことがわかってきた[14].当初,ディスインテグリン様の構造をもつと考えられていたADAMTSファミリー蛋白質のDドメインは,ADAMフ

ファミリー蛋白質のDドメインではなくCドメインのC_bサブドメインと同じ構造をもつこと，さらに興味深いことに，そのC_bサブドメインのMドメインとの相対位置が，ADAMファミリー蛋白質とはまったく異なることがわかったのである（図4a）．さらに，ADAMTSファミリー蛋白質では超可変領域が触媒部位に結合する基質に対して切断部位のすぐC末端側の下流に連続して位置し，エキソサイトとしての機能が強く示唆された[6,14]（図4b）．最近，フォンビルブランド因子切断プロテアーゼであるADAMTS13において，超可変領域のアミノ酸残基の変異により基質の切断活性が低下することが示され，超可変領域が基質認識に直接に関与することがはじめて実験的に示された[15]．

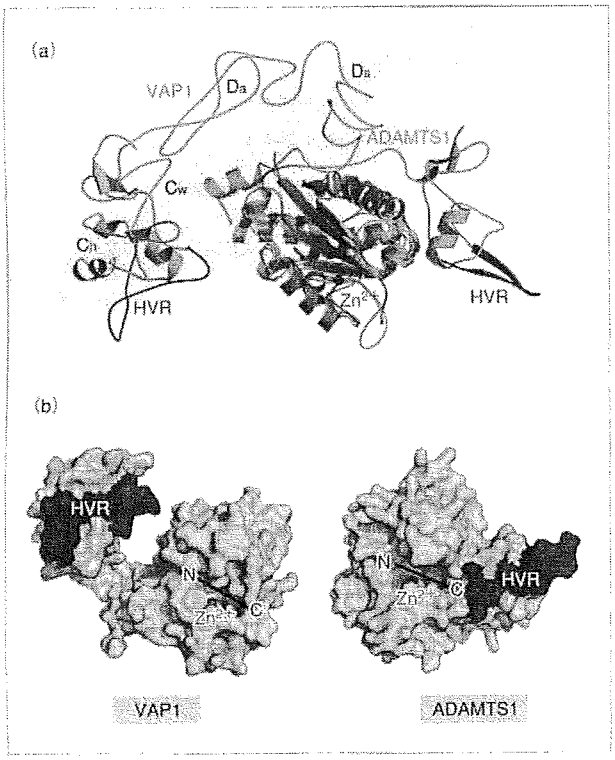

図4　ADAMTS1とVAP1の結晶構造の比較．

(a) ADAMTS1（ピンク色）とVAP1（水色）のMドメインとを重ね合わせた図．ADAMTSのMドメインにつづくDドメイン（黄緑色）は，ADAMファミリー蛋白質のDドメインではなくC_bサブドメインと同じ基本骨格をもつが，ADAMファミリー蛋白質のC_bサブドメインとはMドメインに対する相対位置がまったく異なっていた．

(b) VAP1とADAMTS1の表面モデル．超可変領域を青色，Zn^{2+}を赤色の球で，基質のポリペプチド鎖の結合の向きをN→Cの矢印で示す．ADAMファミリー蛋白質では結合基質のN末端側に，ADAMTSファミリー蛋白質ではC末端側に，超可変領域があった．ADAMTSファミリー蛋白質において，超可変領域は基質切断部位のC末端側を認識するエキソサイトである可能性が示唆された．

HVR：超可変領域．

II RVV-Xの結晶構造と基質認識機構

インドや東南アジアに生息するラッセルクサリヘビ（*Daboia russelli*）の毒は強力な血栓形成作用をもつ．その作用は，この蛇毒に含まれるRVV-X（Russell's viper venom factor X activator）が血液凝固第X因子を活性化することで血中に大量のトロンビンを産生し，宿主が制御不能な速度で血栓形成を進行させることによる．RVV-Xの結晶構造は，ADAMファミリー蛋白質がどのように基質を認識し切断するか，という問題に興味深い示唆をあたえた[16]．

RVV-XはP-Ⅳ型蛇毒メタロプロテアーゼであり，Mドメイン，Dドメイン，Cドメインをもつ重鎖と，2つのC型レクチン様構造をもつ軽鎖からなる（図1，および，図5a）．軽鎖Aの末端システイン残基は重鎖Cドメインの超可変領域にあるシステイン残基とジスルフィド結合を形成し，超可変領域が軽鎖との接触面を形成していた．軽鎖はハブ（*Trimeresurus flavoviridis*）などの毒に含まれる血液凝固因子結合蛋白質[8]と非常に似た構造をもつ．これらの血液凝固因子結合蛋白質は，IX因子あるいはX因子のN末端部位にあるγ-カルボキシルグルタミン酸残基に富むGlaドメインに結合し，それらのリン脂質膜への結合を拮抗的に阻害することで凝固カスケードの増幅を阻止する[8,17]．

構造の類似性から，RVV-Xは2つの軽鎖のあいだのくぼみでX因子のGlaドメインをエキソサイトとして認識する可能性が強く示唆された．X因子は，トリプシンなどほかのセリンプロテアーゼと同様にプロテアーゼによる切断をうけ，新たに生じるN末端（ここでは，Ile195）のアミノ基が蛋白質の内部にたたみこまれることで触媒活性中心が形成され，活性化状態に遷移する（図5b）．RVV-Xは生理的な凝固カスケードでの活性化と同じ部位（Arg194-Ile195結合）を認識・切断しX因子を活性化する．それぞれの蛋白質がもつ可動性を考慮すると，Xa因子の立体構造はRVV-Xの立体構造の凹凸にうまくドッキングし，触媒部位と6.5 nm離れて存在するエキソサイトの存在がRVV-Xに非常に高い基質特異性をあたえると解釈することができた[16]（図5c）．このモデルは，これまで得られている知見をすべて説明することができた．RVV-Xの軽鎖は，ほかの蛇毒類似蛋白質と同様にドメインスワッピング[8]によりGlaドメイン結合性を獲得したと考えられるが，さらに，Mドメイン，Dドメイン，Cドメインをもつメタロプロテアーゼの超可変領域と結合することで高い基質特異性をもつ酵素として分子進化

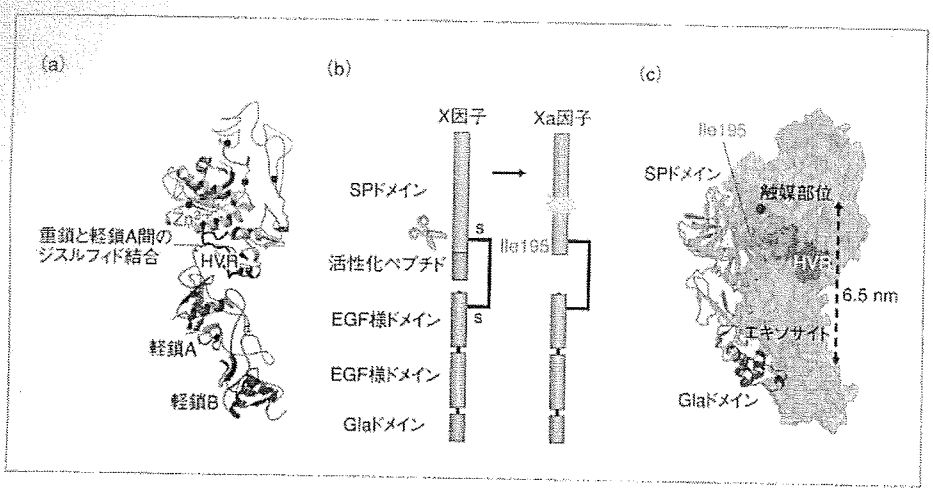

図5 RVV-Xの結晶構造とX因子の活性化機構.

(a) RVV-Xの結晶構造．超可変領域（HVR）が軽鎖Aとのジスルフィド結合を含む接触面を形成していた．
(b) X因子の活性化機構の模式図．生理的な凝固カスケードあるいはRVV-Xの作用によってX因子の活性化ペプチドは切断され，活性化したXa因子となる．
(c) RVV-X（表面表示）とXa因子（リボンモデル）とのドッキングモデル．RVV-Xでは，触媒部位と6.5 nm離れて存在する2つの軽鎖のあいだのくぼみがエキソサイトとしてX因子のGlaドメインを認識し，高い基質認識性を発揮しているものと考えられた．
SPドメイン：セリンプロテアーゼドメイン．

したと考えられた．RVV-XによるX因子の切断機構は，膜型ADAMファミリー蛋白質においても，図3(b)に示すような，第3の蛋白質を介した基質認識機構の存在する可能性を示唆した．

おわりに

本稿では，筆者らの蛇毒ホモログ蛋白質の構造解析の結果を中心に，ADAMファミリー蛋白質について，最近，得られている構造生物学的な知見を紹介した．ADAMファミリー蛋白質はさまざまな膜蛋白質のシェディングに関与するが，多くの場合において，生理的な基質が何であるか，それがどのように識別されているか，というような基本的なことすらわかっていないのが現状である．研究のむずかしさの理由のひとつには，膜構造に組み込まれた酵素と基質との反応である点があげられる．筆者らは，材料が比較的入手しやすく，安定で結晶化に適している点以外に，可溶性プロテアーゼとして機能する点において蛇毒ホモログに注目し研究を行なってきた．すなわち，RVV-Xのように基質が明確で溶液中で酵素反応が速度論的に進む系から，膜型ADAMファミリー蛋白質の基質認識機構の手掛かりを得られるのでは，との期待である．しかし，膜型ADAMファミリー蛋白質と基質とのそれぞれの可溶性部位どうしの反応では切断の再現されないことが多く，細胞膜での反応の理解には，ADAMファミリー蛋白質および基質の双方の，脂質ラフトへの集積，細胞内での局在化など，別の要因の検討も必要であることが指摘されている．また，ADAMファミリー蛋白質と基質とを仲介する蛋白質の候補があがっているが，今後，そのような蛋白質との複合体の構造が解明されることなどより，ADAMファミリー蛋白質の基質認識機構の理解が飛躍的に進むことを期待したい．

文 献

1) Blobel, C. P. *et al.*: *Nature*, **356**, 248-252 (1992)
2) Edwards, D. R., Handsley, M. M., Pennington, C. J.: *Mol. Aspects Med.*, **29**, 258-289 (2009)
3) Wolfsberg, T. G. *et al.*: *Dev. Biol.*, **169**, 378-383 (1995)
4) Black, R. A. *et al.*: *Nature*, **385**, 729-733 (1997)
5) Moss, M. L. *et al.*: *Nature*, **385**, 733-736 (1997)
6) Takeda, S.: *Semin. Cell Dev. Biol.*, **20**, 146-152 (2009)
7) Fox, J. W., Serrano, S. M.: *FEBS J.*, **275**, 3016-3030 (2008)
8) 山崎泰男・森田隆司: 蛋白質 核酸 酵素, **54**, 628-634 (2009)
9) Takeda, S., Igarashi, T., Mori, H., Araki, S.: *EMBO J.*, **25**, 2388-2396 (2006)
10) Igarashi, T., Araki, S., Mori, H., Takeda, S.: *FEBS Lett.*, **581**, 2416-2422 (2007)
11) Fujii, Y. *et al.*: *J. Mol. Biol.*, **332**, 1115-1122 (2003)
12) Takagi, J.: *Curr. Opin. Cell Biol.*, **19**, 557-564 (2007)
13) Janes, P. W. *et al.*: *Cell*, **123**, 291-304 (2005)
14) Gerhardt, S. *et al.*: *J. Mol. Biol.*, **373**, 891-902 (2007)
15) de Groot, R. *et al.*: *Blood*, **113**, 5609-5616 (2009)
16) Takeda, S., Igarashi, T., Mori, H.: *FEBS Lett.*, **581**, 5859-5864 (2007)
17) Mizuno, H., Fujimoto, Z., Atoda, H., Morita, T.: *Proc. Natl. Acad. Sci. USA*, **98**, 7230-7234 (2001)

武田壮一

略歴：1996年 名古屋大学大学院理学研究科博士課程 満期修了，同年 松下電器国際研究所 リサーチアソシエイト，1997年 博士（理学），1998年 科学技術振興事業団 さきがけ研究員，2000年 理化学研究所 研究員を経て，2003年より国立循環器病センター研究所 室長．

研究テーマ：モジュラー蛋白質，蛋白質複合体の立体構造と作用機構の解明．

血栓止血誌 20(3)：307～314, 2009

◆総　説◆

蛇毒メタロプロテアーゼの立体構造とラッセルクサリヘビ毒素によるX因子活性化機構

武田　壮一

武田壮一

1991年3月　名古屋大学理学部生物学科卒業
1996年7月　名古屋大学大学院理学研究科博士課程満期修了
1996年8月　松下電器産業(株)国際研究所リサーチアソシエイト
1997年7月　博士（理学）取得
1998年10月　科学技術振興事業団さきがけ研究「形とはたらき」領域研究員
2000年1月　理化学研究所構造生物化学研究室研究員
2003年1月　国立循環器病センター研究所心臓生理部室長
現在に至る

Crystal structures of snake venom metalloproteinases and the molecular mechanism of factor X activation by Russell's viper venom

Soichi TAKEDA

Key words: snake venom metalloproteinase, crystal structure, ADAM/ADAMTS proteinase, factor X activator

1. はじめに

クサリヘビ科（Viperidae）に属する毒蛇の毒液には様々なタンパク性の生理活性成分が含まれ，これらは獲物の体内で標的タンパク質と相互作用し，出血，壊死，浮腫，血栓形成，血圧降下などを引き起こし致死的な危害を与える．蛇毒からは血小板フィブリノーゲン/VWF受容体αIIbβ3インテグリンに結合するディスインテグリン，血漿タンパク質や血小板膜糖タンパク質などに結合するC型レクチン様タンパク質(CLP)，トロンビン様セリンプロテアーゼ，など血液凝固阻害あるいは活性化因子として働く様々なタンパク質が単離され，その標的タンパク質に対する特異性の高さからこれまで血栓止血研究において大きな貢献をしてきた．これら蛇毒分子のいくつかについては本誌を含め既に詳しく解説されているので参照して頂きたい[1)-6)]．トロンビンをはじめ生理的な凝固カスケードに関わる血漿因子群が総じて触媒活性基としてセリンを有するセリンプロテアーゼであるのに対し，出血性蛇毒には触媒部位に亜鉛イオンを含むメタロプロテアーゼ（snake venom metalloproteinase：SVMP）を多く含むのが特徴である．特に高分子量（分子量約4万ダルトン以上）で複数のドメインを有するSVMPは高い出血活性や，高い基質特異性を持つものが多く，また一方でヒトを含む哺乳動物の膜結合プロテアーゼやvon Willebrand因子（VWF）切断酵素ADAMTS13などとの相同性を示すことから興味が持たれている．本稿ではこれら高分子量SVMPについて最近得られた構造生物学的知見，特に哺乳動物プロテアーゼADAMおよびADAMTSとの関係を前半で，後半で高分子量SVMPの中でも特にユニークな立体構造と作用機構を有するラッセルクサリヘビ毒由来X因子活性化酵素（RVV-X）について紹介したい．

2. 蛇毒メタロプロテアーゼと哺乳動物ADAM・ADAMTS

マムシやハブの毒成分の内，末梢血管を破壊し赤血球を血管外に漏出させる出血因子の正体がSVMPであり，致死因子の本体と考えられてい

国立循環器病センター研究所心臓生理部〔〒565-8565 大阪府吹田市藤白台5-7-1〕
Department of Cardiac Physiology, National Cardiovascular Center Research Institute
〔5-7-1 Fujishiro-dai, Suita, Osaka 565-8565, Japan〕
Tel: 06-6833-5012　Fax: 06-6835-5416　E-mail: stakeda@ri.ncvc.go.jp